UNIVERSIDAD NACIONAL AUTÓNOMA DE MÉXICO
POSGRADO EN CIENCIAS FÍSICAS
INSTITUTO DE FÍSICA
INSTITUTO DE CIENCIAS FÍSICAS
FÍSICA DE ALTAS ENERGÍAS, FÍSICA NUCLEAR, GRAVITACIÓN Y FÍSICA MATEMÁTICA

Holographic dark energy: a fundamental alternative

TESIS
QUE PARA OPTAR POR EL GRADO DE:
MAESTRO EN CIENCIAS (FÍSICA)

PRESENTA:
MIGUEL ALFONSO ZAPATA DE LA CRUZ

TUTOR PRINCIPAL
DR. JOSÉ ALBERTO VÁZQUEZ GONZÁLEZ (ICF-UNAM)
MIEMBROS DEL COMITÉ TUTOR
DRA. MARIANA VARGAS MAGAÑA (IF-UNAM)
DR. SEBASTIEN FROMENTEAU (ICF-UNAM)

CIUDAD DE MÉXICO, MÉXICO, NOVIEMBRE DEL 2024

UNIVERSIDAD NACIONAL AUTÓNOMA DE MÉXICO
PROGRAMA DE POSGRADO EN CIENCIAS FÍSICAS

ACTA DE GRADO

No. de cuenta
523011369

En la Universidad Nacional Autónoma de México, **a través de un AULA VIRTUAL UNIVERSITARIA,** a las **10:00** horas del día 02 de diciembre de 2024, el alumno de nacionalidad **mexicana**

MIGUEL ALFONSO ZAPATA DE LA CRUZ

cuya fotografía aparece al margen, se presentó con el fin de sustentar el examen para obtener el grado de

MAESTRO EN CIENCIAS (FÍSICA)

en la modalidad de graduación por **TESIS,** con el trabajo titulado: **"Holographic dark energy: A fundamental alternative",** del cual fue tutor principal el **DR. JOSÉ ALBERTO VÁZQUEZ GONZÁLEZ.**

El alumno cursó sus estudios en el período **2023-1** a **2024-2**, obtuvo un promedio de **9.90** y cumplió con los requisitos académicos señalados en el plan de estudios **4204** aprobado por el Consejo Universitario.

El jurado resolvió otorgarle la calificación de

le hizo saber el resultado de su examen y le tomó la Protesta Universitaria.

El jurado estuvo integrado por:

Presidente: Dr. Alejandro Avilés Cervantes
Secretario: Dr. José Alberto Vázquez González
Vocal 1: Dr. Marcos Alejandro García García
Vocal 2: Dr. Miguel Ángel Cruz Becerra
Vocal 3: Dr. Josué De Santiago Sanabria

PRESIDENTE DEL JURADO **SECRETARIO DEL JURADO**

VOCAL 1 DEL JURADO **VOCAL 2 DEL JURADO** **VOCAL 3 DEL JURADO**

El suscrito coordinador del programa constató que las firmas corresponden al jurado designado

"POR MI RAZA HABLARÁ EL ESPÍRITU"
DR. ALBERTO GÜIJOSA HIDALGO
COORDINADOR DEL PROGRAMA

No. Folio del Programa
4205070012468

PROTESTA UNIVERSITARIA DE INTEGRIDAD Y HONESTIDAD ACADÉMICA Y PROFESIONAL
(Graduación con trabajo escrito)

De conformidad con lo dispuesto en los artículos 87, fracción V, del Estatuto General, 68, primer párrafo, del Reglamento General de Estudios Universitarios y 26, fracción I, y 35 del Reglamento General de Exámenes, me comprometo en todo tiempo a honrar a la Institución y a cumplir con los principios establecidos en el Código de Ética de la Universidad Nacional Autónoma de México, especialmente con los de integridad y honestidad académica.

De acuerdo con lo anterior, manifiesto que el trabajo escrito titulado:

Holographic dark energy: a fundamental alternative

que presenté para obtener el grado de -----Maestria----- es original, de mi autoría y lo realicé con el rigor metodológico exigido por mi programa de posgrado, citando las fuentes de ideas, textos, imágenes, gráficos u otro tipo de obras empleadas para su desarrollo.

En consecuencia, acepto que la falta de cumplimiento de las disposiciones reglamentarias y normativas de la Universidad, en particular las ya referidas en el Código de Ética, llevará a la nulidad de los actos de carácter académico administrativo del proceso de graduación.

Atentamente

Miguel Alfonso Zapata de la Cruz
Cuenta: 523011369

(Nombre, firma y Número de cuenta de la persona alumna)

1. Datos del alumno
Miguel Alfonso Zapata De la Cruz
Universidad Nacional Autónoma de México
Instituto de Física
Instituto de Ciencias Física
Maestría en Ciencias (Física)
#523011369

c2. Datos del tutor (sinodal 1)
Dr. José Alberto Vázquez González
Universidad Nacional Autónoma de México
Instituto de Ciencias Física
3. Datos de sinodal 2
Dr. Alejandro Avilés Cervantes
Universidad Nacional Autónoma de México
Instituto de Ciencias Física

4. Datos de sinodal 2
Dr. Marcos Alejandro García García
Universidad Nacional Autónoma de México
Instituto de Física

5. Datos del sinodal 3
Dr. Josué De Santiago Sanabria
Centro de Investigación y de Estudios Avanzados del Instituto Politécnico Nacional
Departamento de Física

6. Datos del sinodal 4
Dr. Miguel Ángel Cruz Becerra
Universidad Veracruzana
Facultad de Física

This work is dedicated to one of the biggest headaches for cosmologists today. However, despite this and other efforts, *the nature of dark energy is still dark.*

Investigación realizada gracias al Programa de Apoyo a Proyectos de Investigación e Innovación Tecnológica PAPIIT IN117723-UNAM y por medio del apoyo FORDECYT-PRONACES/304001/202.

Agradecimientos

En primer lugar, agradezco especialmente a mi asesor de tesis, el Dr. José Alberto Vázquez, quien por medio de su invaluable guía y apoyo a lo largo de este proceso, ha alimentado mi ambición por entender nuestro universo. Su paciencia, y generosidad al compartir su conocimiento me han permitido crecer académica y personalmente, lo cual me hace sentir afortunado de haber tenido mi primer contacto con la cosmología bajo su supervisión.

De igual forma, agradezco a la Dra. Gabriela García por compartir sus conocimientos, su entusiasmo y brindar aportaciones significativas a este trabajo. Sin embargo, agradezco aún más su amistad y paciencia durante este proceso.

A los profesores e investigadores que conforman el jurado de este trabajo, por invertir su tiempo y compartir sus comentarios, los cuales fueron crucial para enriquecer la calidad de esta tesis.

A todos los nuevos amigos y amigas que tuve el placer de conocer durante la maestría. Entre ellos destacan Hugo, Rafa, Yusef, Luis E., Juan, Jimena y Donaldo, quienes siempre estuvieron cuando más lo necesite y con algunos compartí noches estresantes de exámenes o interminables tareas.

En especial, este trabajo es dedicado con todo el amor a mis padres, por su amor y apoyo incondicional, creyendo siempre en mí, incluso en los momentos más difíciles. Sin su aliento y comprensión, no hubiera sido posible alcanzar esta meta. A Tania, quien ha sido un apoyo indispensable durante este proceso. Ella ha sido siempre un refugio, creyendo siempre en mí, incluso cuando yo he dudado de mí mismo.

Finalmente, agradezco a la Universidad Nacional Autónoma de México que, por medio del posgrado en ciencias físicas, me ha formado académicamente. Al Consejo Nacional de Humanidades, Ciencias y Tecnologías (CONAHCyT) por el apoyo durante mis estudios de maestría. Sin estos importantes organismos, este trabajo hubiera sido simplemente irrealizable.

Resumen

En esta tesis, realizamos un estudio sobre el panorama actual de la energía oscura holográfica y sus implicaciones al compararla con datos observacionales. La energía oscura es un misterioso componente del universo que constituye aproximadamente el 68% de su contenido total, según las observaciones astronómicas. La necesidad de introducir este componente se debe a la explicación de la expansión acelerada de nuestro universo según las observaciones. A diferencia de la materia oscura, que ejerce atracción gravitacional, la energía oscura parece tener un efecto repulsivo, actuando como una especie de fuerza antigravitatoria que causa la expansión acelerada del espacio-tiempo. Por esta razón, en esta tesis se realizó una revisión de los aspectos básicos de la cosmología y los aspectos observacionales que dan lugar a la necesidad de la energía oscura. De igual forma, se aborda la necesidad de introducir un término de constante cosmológica como primer candidato de este ente. Sin embargo, este modelo presenta discrepancias o tensiones que nos permiten imaginar su incompletitud y, por lo tanto, introducir modelos extendidos de energía oscura. En este caso, la energía oscura holográfica.

Para introducir esta alternativa fundamental, se estudiaron las ideas que dieron lugar al principio holográfico a partir de la fórmula de Bekenstein-Hawking. Esta fórmula nos indica que la información de la entropía dentro de un volumen específico en un espacio determinado puede ser deducida a partir de la información que se puede codificar sobre la frontera de esa región. La extrapolación de esta idea a la teoría cuántica de campos, dio lugar a lo que hoy conocemos como principio holográfico. Al utilizar este resultado en teoría cuántica de campos para la densidad de energía del vacío y compararlo con la energía oscura presente en nuestro universo, es posible encontrar la ecuación que indica la evolución de la energía oscura.
Debido a que este modelo se caracteriza por la entropía asociada, es posible construir nuevos mod-

elos de energía oscura al usar entropías más generales. En esta tesis, exploramos uno las versiones generalizadas de este modelo, por medio de introducir nuevas entropías, en este caso las de Tsallis, Barrow y modelos de exponentes generalizados donde no necesariamente es constante, lo que da lugar a densidades de energía con parámetros adicionales que, en el límite adecuado, reproducen la energía oscura estándar y ΛCDM. Además, de esta extensión, estudiamos de forma breve algunos otras posibilidades como lo son la interacción entre materia oscura y energía oscura holográfica, la presencia de un universo con curvatura espacial, la teoría de perturbaciones en el modelo de energía oscura holográfica y la dependencia temporal de la constante de Newton en este modelo. Finalmente, llevamos a cabo una inferencia de los parámetros cosmológicos y los parámetros adicionales de cada modelo utilizando la inferencia bayesiana y datos observacionales de supernovas, oscilaciones acústicas de bariones y cronómetros cósmicos, a través de la paquetería en Python, Simplemc. Pudimos determinar qué modelo se ajusta mejor a los datos al comparar la evidencia bayesiana y el término χ^2 , así como la información cosmológica adicional proporcionada por los modelos holográficos en comparación con ΛCDM.

Abstract

In this thesis, we studied the current landscape of holographic dark energy and its implications compared to observational data. According to astronomical observations, dark energy is a mysterious component of the universe that constitutes approximately 68% of its total content. The need to introduce this component arises from the explanation of the accelerated expansion of our universe as observed. Unlike dark matter, which exerts gravitational attraction, dark energy seems to have a repulsive effect, acting as a sort of anti-gravitational force that drives the expansion of spacetime. For this reason, this thesis undertook a review of the basic aspects of cosmology and the observational aspects that give rise to the need for dark energy. Similarly, it addresses the need to introduce a cosmological constant term as the first candidate for this entity. However, this model presents discrepancies or tensions that allow us to imagine its incompleteness and, therefore, introduce extended models of dark energy. In this case, holographic dark energy.
To introduce this fundamental alternative, we studied the ideas that gave rise to the holographic principle from the Bekenstein-Hawking formula. This formula indicates that the entropy information within a specific volume in a given space can be deduced from the information that can be encoded on the boundary of that region. The extrapolation of this idea to quantum field theory gave rise to what we know today as the holographic principle. By using this result in quantum field theory for the energy density of the vacuum and comparing it with the dark energy present in our universe, it is possible to find the equation indicating the evolution of dark energy.

Because this model is characterized by the associated entropy, it is possible to construct new dark energy models by using more general entropies. In this thesis, we explore one of the generalized versions of this model, by introducing new entropies, in this case, those of Tsallis, Barrow, and generalized exponent models where it is not necessarily constant, resulting in energy densities with

additional parameters that, in the right limit, reproduce the energy of the dark energy and the ΛCDM model. In addition to this extension, we briefly study some other possibilities such as the interaction between dark matter and holographic dark energy, the presence of a spatially curved universe, the perturbation theory in the holographic dark energy model and the time dependence of Newton's constant in this model.

Finally, we performed inference of the cosmological parameters and additional parameters of each model using Bayesian inference and observational data from supernovae, baryon acoustic oscillations, and cosmic chronometers, via the Python package, SimpleMC. We were able to determine which model best fits the data by comparing the Bayesian evidence and the χ^2 term, as well as the additional cosmological information provided by the holographic models compared to ΛCDM.

Contents

List of Figures

Chapter 1

Introduction to Cosmology

1.1 General relativity

In 1915, Albert Einstein put forward an idea that would revolutionize, once and for all, how we would think about gravity and the structure of the universe. He laid out a new theory of gravity that, for the first time in centuries, moved beyond the work of Isaac Newton. This is a general theory in which one can describe gravitational force, apart from the Newtonian paradigm that preceded it. In such a way, Einstein's field equations explain the relationship between matter and energy and spacetime curvature. Solutions to such equations yield groundbreaking predictions confirmed by vast experimental observations.

1.1.1 Equivalence principle

One of the most revolutionary principles in physics, allowing us to understand the connection between the mass of a body and the force of gravity, is the principle of equivalence in general relativity or the equivalence principle of Einstein. The first variant of this principle was called the "weak equivalence principle," postulated by Galileo and Newton. The original form of this makes the statement that inertial mass "m" is equal to gravitational mass "M" [1]. These masses are the ones that come into the expressions of the force.

$$\vec{f} = m\vec{a}, \tag{1.1}$$

$$\vec{f} = -M\nabla\phi, \tag{1.2}$$

with ϕ is the gravitational potential. However, all experiments have shown no distinction between these masses, i.e. $m = M$. From these equations, notice that the direct consequence is

$$\vec{a} = \ddot{\vec{x}} = -\nabla\phi(\vec{x}), \tag{1.3}$$

This indicates that the motion of particles in free fall is universal.

1.1.2 The metric

For a theory that can describe gravity in curved spaces, a general metric $g_{\mu\nu}$ is necessary, which, in some limits, can reproduce the metric of a flat Minkowski space $\eta_{\mu\nu}$. Rather than conceptualizing gravity as an external force and describing particles navigating a gravitational field, we can integrate gravity into the metric [2]. This idea allows us to discuss particles moving unhindered in a distorted or curved space-time, where the metric cannot be uniformly transformed into Euclidean form throughout. In a four space-time dimensions the interval or the *invariant* for four-vectors (x_0, x_1, x_2, x_3) is

$$ds^2 = g_{\mu\nu}dx^\mu dx^\nu. \tag{1.4}$$

Where the Greek indices μ and ν range from 0 to 3, and we use Einstein's summation convention. Notice that the first component is the time-like coordinate ($dx^0 = dt$) and the last three are spatial coordinates. The metric $g_{\mu\nu}$ has four diagonal and six off-diagonal components and, thus, is symmetric. In the special relativity case, the space is described by the Minkowski metric

$$\eta_{\mu\nu} = Diag(1, -1, -1, -1). \tag{1.5}$$

In the following sections, we will know the metric that describes de expansion of the Universe.

1.1.3 Einstein Equations

The field equations of Einstein are the cornerstones of modern physics, these were formulated in the early years of the 20th century. Starting from this, Einstein immediately began to develop a theory that combined gravity with his work [3].
The most fundamental aspect of general relativity consists of the fact that this theory has encoded in it a way to represent gravitation in terms of a metric. Another very important aspect of the theory relates this metric to the matter and energy distributed in the universe. That aspect is encoded in Einstein's equations, which relate components of Einstein's tensor describing geometry to the energy-momentum tensor defining energy distribution, i.e.

$$G_{\mu\nu} \equiv R_{\mu\nu} - \frac{1}{2} g_{\mu\nu}\mathcal{R} = \frac{8\pi G}{c^4} T_{\mu\nu}. \tag{1.6}$$

In this equation, $G_{\mu\nu}$ is the Einstein tensor, $R_{\mu\nu}$ is the Ricci tensor given by

$$R_{\mu\nu} = \Gamma^{\alpha}_{\mu\nu,\alpha} - \Gamma^{\alpha}_{\mu\alpha,\nu} + \Gamma^{\alpha}_{\beta\alpha}\Gamma^{\beta}_{\mu\nu} - \Gamma^{\alpha}_{\beta\mu}\Gamma^{\beta}_{\alpha\nu}, \tag{1.7}$$

with $\Gamma^{\alpha}_{\mu\nu}$ are the Christoffel symbols.

Also, in the Einstein equations is present the Ricci scalar is just given by $\mathcal{R} = g^{\mu\nu}R_{\mu\nu}$, and the energy-momentum for a perfect fluid is

$$T^{\mu\nu} = \begin{pmatrix} \rho c^2 & 0 & 0 & 0 \\ 0 & p & 0 & 0 \\ 0 & 0 & p & 0 \\ 0 & 0 & 0 & p \end{pmatrix}. \tag{1.8}$$

Notice that the Einstein equation expresses the dynamic interplay between mass and energy and space-time geometry.

But this is important not only for the aesthetic value of the Einstein equation but also for its predictive power: From this theory, a perspective can be given from which many gravitational phenomena can be understood, such as the motion of the planets and light bending by gravitational fields. Most remarkably, it predicted gravitational wave ripples in the fabric of space-time. The detection of these gravitational waves in 2015 confirmed one of the last untested predictions of Einstein's theory and proof that black holes exist in our universe.

However, the implications of Einstein's equation extend far beyond the fields of astrophysics and cosmology: the truth is that it is supposed to give a kind of shock to mankind's knowledge concerning the origin, evolution, and ultimate fate of the universe. Cosmological models attempt to describe the history of the universe from a primeval beginning to the present structure, such as the Big Bang Theory. Einstein's equation has been that from which modern theories of gravitation are derived, and it has been a kind of wellspring for generations of physicists interested in pushing the frontiers of both theoretical and experimental physics. From the mystery of black holes to the search for a united theory of fundamental forces, the Einstein equation continues to be a powerful driving force in scientific research and exploration.

In recent decades, cosmology has had an essential role in the scientific environment due to increasingly precise observations that allow us to know the universe in which we live in an increasingly detailed way. The observation that would start this revolution in contemporary cosmology, besides paralyzing the world of science, occurred in 1998 when Riess from the High-redshift Supernova Search Team and Perlmutter from the Supernova Cosmology Project Team independently reported the accelerated expansion of the universe.

Since these results, many proposals have emerged to explain this phenomenon. However, using observational data, two proposals can answer one of the most critical questions: *what causes the universe's accelerated expansion?* These proposals are Modified Gravity and *Dark Energy.*

1.2 Historical Context

The roots of cosmology stretch back to antiquity, where early civilizations crafted intricate cosmological narratives to explain the origin and nature of the universe. In Mesopotamia, the Babylonians envisioned a cosmos governed by divine order, with celestial bodies serving as omens and symbols of cosmic harmony. The Egyptians developed cosmological myths centered around the sun god Ra, whose journey across the sky represented the cycle of life, death, and rebirth [4].
Pythagoras, Plato, and Aristotle sought to understand the universe through reason and observation. Pythagoras suggested that there existed a basic mathematical harmony in the universe, and

Plato envisioned an independent, transcendental realm of ideal forms beyond the material world. In Aristotle's cosmology, the center was occupied by Earth, with celestial spheres rotating around it thereby laying the foundation for centuries of cosmological thought based on anthropocentrism.

1.2.1 The Ptolemaic Universe

The Ptolemaic model of Claudius Ptolemy in the 2nd century CE was the climax of ancient cosmology. Elaborating on what Aristotle had previously laid down, Ptolemy described a geocentric universe where Earth was at the center and the rest of the celestial bodies orbited it along perfect circles, as shown 1.1 below. To explain the observed retrograde motion of the planets while still holding on to perfection for the geocentric heaven, epicycles, and referents were incorporated into the analysis.

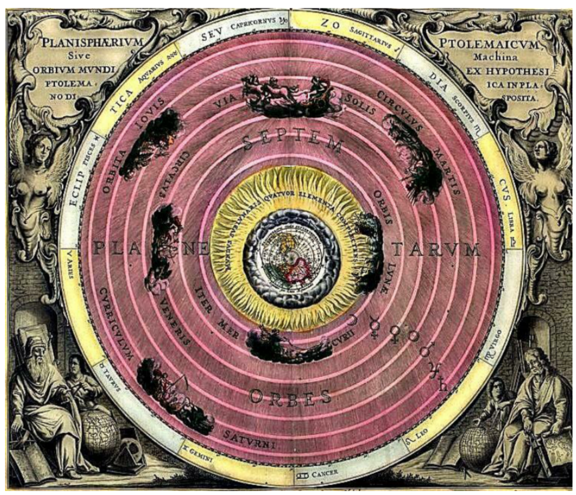

Figure 1.1: A Ptolemaic map of the world, created by Andreas Cellarius in 1708.

1.2.2 Copernican principle

In the 16th century, Nicolaus Copernicus proposed one of the backbones of modern cosmology. This idea is known as *the Copernican Principle*. This idea changed the perspective of humanity about the relation to the cosmos and our role in it, instead, it asserts that the laws of physics and the universe's properties are uniform and independent of any particular vantage point [5]. In this way, Nicolaus Copernicus challenged the traditional geocentric model, which considers that the Earth is the center of the universe, thus, the sun and other planets orbit around it. This paradigm shift not only transformed our understanding of planetary motion but also laid the groundwork for the Copernican Principle, which asserts the absence of privileged positions in the universe. This principle can be summarized as follows [6]

"On the Earth or in the Solar System, are not privileged observers of the universe".

Observations in astronomy throughout history, support the Copernican Principle. Surveys of distant galaxies, cosmic microwave background radiation, and the large-scale distribution of matter all point to a vast, uniform universe devoid of privileged locations. The cosmic microwave background, in particular, serves as a relic of the early universe, offering insights into its fundamental properties and evolution [7].

1.3 Cosmology

1.3.1 Isotropy and homogeneity

The vast expanse of galaxies, stars, and cosmic structures within the universe has perpetually captivated humanity with its intricate beauty and complexity. The fundamental concepts of isotropy and homogeneity are foundational in comprehending the universe's structure. These concepts, rooted in cosmology, provide crucial insights into the universe's large-scale properties and evolution over time. This chapter explores the profound significance of isotropy and homogeneity (see figure 1.2), delving into their definitions, implications, and the evidence supporting their validity [8].

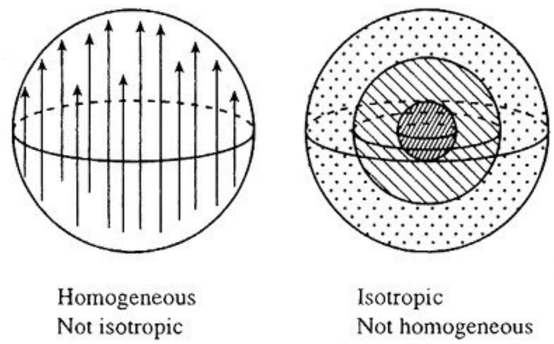

Figure 1.2: Homogeneity and isotropy diagram [9]

Firstly, the *isotropy* refers to the uniformity of the universe's properties in all directions. In an isotropic universe, observational data should not exhibit preferential directions or orientations; instead, they should appear statistically identical regardless of the observer's location or perspective.

In the same way, the *homogeneity* denotes the uniform distribution of matter and energy throughout the universe on large scales. When observed on sufficiently large scales, a homogeneous universe exhibits a consistent density of cosmic structures, such as galaxies and galaxy clusters. This uniformity implies that the universe looks the same from any vantage point, without distinct regions of higher or lower density.

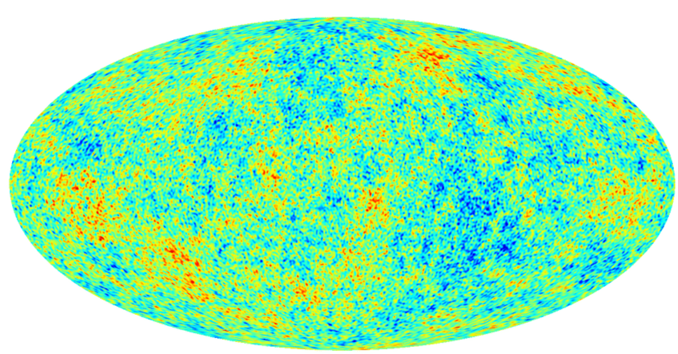

Figure 1.3: Anisotropies of the Cosmic Microwave Background, the colors represent temperature's difference map [10].

The homogeneity and isotropy in the Cosmic Microwave Background (CMB) provide compelling evidence for the cosmological principle, as shown in the figure 1.3. Observations of the CMB reveal a remarkably uniform temperature distribution across the sky, with temperature fluctuations at the level of one part in a hundred thousand. This uniformity suggests that the universe possesses a high degree of homogeneity on large scales, consistent with the predictions of the cosmological principle.

1.4 Friedmann-Lemaître-Robertson- Walker

The Friedmann-Lemaître-Robertson- Walker (FLRW) metric is a solution to Einstein's field equations of general relativity and describes the geometry of a homogeneous, isotropic, and expanding universe [11]. It encompasses three key components: homogeneity, isotropy, and cosmic expansion.

The FLRW metric embodies the principles of the Cosmological Principle by providing a mathematical framework that describes a universe consistent with its assumptions. It allows cosmologists to model the universe's evolution and predict its properties based on observations. One of the remarkable implications of the FRW metric and the cosmological principle is the prediction of phenomena such as the redshift of distant galaxies and the CMB. Observations of the CMB, in particular, have provided compelling evidence for the isotropy and homogeneity of the universe, consistent with the predictions of the FRW metric and the Cosmological Principle.

The invariant element in this universe is

$$ds^2 = c^2dt^2 - a^2(t)\left(\frac{dr^2}{1-k\left(r/R_0\right)^2} + r^2\left(d\theta^2 + \sin(\theta)d\phi^2\right)\right), \tag{1.9}$$

where $a(t)$ is the scale factor, R_0 is the radius of the sphere and the constant k involves the following cases

- for $k = -1$, is an open universe.

- for $k = 0$, is a flat universe.

- for $k = 1$, is a closed universe.

The components of the Ricci tensor for a flat universe are (consider $c = 1$)

$$R_{00} = -3\left(\frac{\ddot{a}}{a}\right). \tag{1.10}$$

$$R_{ij} = \left(2\left(\frac{\dot{a}}{a}\right)^2 + \frac{\ddot{a}}{a}\right) g_{ij}. \tag{1.11}$$

From these results, we can find the Ricci scalar, and then calculate the components of the Einstein Equations, thus, taking the first component we get the first Friedmann equation in the form

$$\left(\frac{\dot{a}}{a}\right)^2 = \frac{8\pi G}{3}\rho. \tag{1.12}$$

We need to define the ratio of the rate of change of the scale factor to the current value of the scale factor $a(t)$ or the *Hubble parameter* and the critical density

$$H(t) \equiv \frac{\dot{a}}{a}, \tag{1.13}$$

$$\rho_c \equiv \frac{3H^2}{8\pi G}. \tag{1.14}$$

Where H_0 is the present value of the Hubble parameter [12]

$$H_0 = 100\, h\, km\, sec^{-1} Mpc^{-1} = \frac{h}{0.98 \times 10^{10} years} = 74.2 \pm 3.6\, km\, sec^{-1}\, Mpc^{-1}, \tag{1.15}$$

and the value of the critical density at the present day is

$$\rho_{c,0} = 1.88\, h^2\ \times 10^{-29} g\, cm^3. \tag{1.16}$$

The second Friedmann equation is obtained using the spatial components of the Einstein equations. This equation is

$$\frac{\ddot{a}}{a} = -\frac{4\pi G}{3}\left(\rho + 3P\right). \tag{1.17}$$

From these two equations, we can find the third equation deriving (1.12) with respect to cosmic time and replacing (1.17). The last of the equation is the continuity equation

$$\dot{\rho} + 3H(\rho + p) = 0. \tag{1.18}$$

In cosmology, the continuity equation is applied to various cosmic fluids to study their evolution over cosmic time. For example, it can describe the evolution of dark matter, baryonic matter (ordinary matter), and radiation in the expanding universe. By solving the continuity equation alongside other relevant equations, cosmologists can model the behavior of these cosmic fluids, predict their distributions, and understand their impact on the universe's large-scale structure.

1.5 Components of the universe

To understand the universe's evolution, it is necessary to know its components and dynamics. In cosmology, this entails defining the connection between mass density and pressure, known as the equation of state. Mathematically, this relation is $p = \omega\rho$, where ω is the equation of the state parameter (EoS).
Currently, we will explore some potential scenarios [8].

- **Matter:** In the Cosmology's context, the term *matter* is used for non-relativistic matter. This kind of component is any material that has negligible pressure, i.e., $p = 0$.
  In the case of a universe dominated by non-relativistic matter, from solving the continuity equation (1.18) we get
  $$\rho_m = \rho_{m0} a^{-3}. \tag{1.19}$$
  The scale factor and the Hubble parameter are given by
  $$a(t) = \left(\frac{t}{t_0}\right)^{\frac{2}{3}}, \quad H(t) = \frac{2}{3t}, \tag{1.20}$$
  where t_0 is the present time.

- **Radiation:** For this case the pressure is $p = \rho/3$, in the same way, solving (1.18) for an universe dominated by radiation, we can note

$$\rho_r = \rho_{r0} a^{-4}. \tag{1.21}$$

The scale factor and the Hubble parameter are

$$a(t) = \left(\frac{t}{t_0}\right)^{\frac{1}{2}}, \quad H(t) = \frac{1}{2t}. \tag{1.22}$$

- **Curvature:** To keep the same notation in terms of the energy density, we can define the component associated with the curvature as follows,

$$\rho_k \equiv -\frac{3k}{8\pi G a^2}. \tag{1.23}$$

The EoS associated with the curvature is $\omega = -\frac{1}{3}$. Therefore, for a universe dominated by the curvature, the scale factor and the Hubble parameter are

$$a(t) = \frac{t}{t_0}, \quad H(t) = \frac{1}{t}. \tag{1.24}$$

- **Cosmological constant:** As we will see in chapter 2 with more details, Einstein introduced the cosmological constant Λ to obtain a static universe. In the same way that the curvature case, it is possible to define the dark energy density for the cosmological constant

$$\rho_\Lambda = \frac{\Lambda}{8\pi G}. \tag{1.25}$$

Furthermore, we can consider the cosmological constant associated with the vacuum energy, thus, this is the case of a perfect fluid with negative pressure, i.e., $\omega = -1$. Finally, in the case of a universe dominated by the cosmological constant, we get

$$a(t) \propto e^{\sqrt{\Lambda/3}t}, \quad H(t)\,\text{constant}. \tag{1.26}$$

1.5.1 ΛCDM model

The *standard cosmological model* or Λ Cold Dark Matter (ΛCDM) model is the simplest model that can explain a lot of cosmological observations. Its name is due to some considerations which conform to it. Some of these are,

- Einstein's theory of general relativity is the correct theory to describe gravity on cosmological scales.
- The cosmological principle is valid and establishes that the universe is statistically homogeneous and isotropic on sufficiently large scales.
- The universe is made up of ordinary matter (baryons and leptons), cold dark matter (non-relativistic matter, which only interacts gravitationally), radiation (photons, neutrinos), and the cosmological constant Λ as responsible for the accelerated expansion of the universe.
- In the early universe a primordial phase of inflation occurred, i.e. a period of very rapid acceleration. This is usually assumed in this framework because it solves the flatness problem.

Particularly, in this model due to the cosmological principle, the spatial part of the FRW metric is considered plane, i.e. $k = 0$.

Now, to visualize the evolution of the above quantities, it is convenient to define a new dimensionless density parameter for each component of the universe. The general form is given by

$$\Omega_i(t) \equiv \frac{\rho_i(t)}{\rho_c(t)}, \tag{1.27}$$

with ρ_c as the critical density previously defined. From this new definition, we can express the Friedmann constrain in the form

$$\Omega_\Lambda + \Omega_k + \Omega_m + \Omega_r = 1. \tag{1.28}$$

Another dimensionless quantity that is convenient to define in the context of cosmology is the *redshift* z, in the form

$$1 + z = \frac{a_0}{a(t_1)} \tag{1.29}$$

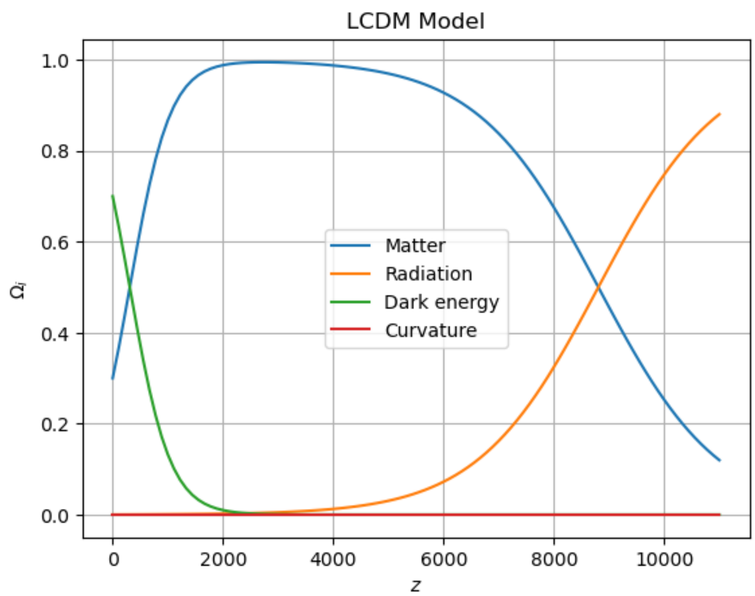

Figure 1.4: Evolution of the dimensionless density parameters.

where a_0 is the scalar factor at the present time ($a_0 = 1$) and $a(t_1)$ is the scalar factor at an arbitrary time t_1.
The Friedmann equation in terms of the dimensionless density parameters and the redshift is

$$H^2(z) = H_0^2 \left(\Omega_{k,0}(z+1)^2 + \Omega_{r,0}(z+1)^4 + \Omega_{m,0}(z+1)^3 + \Omega_{\Lambda,0}\right), \quad (1.30)$$

where $\Omega_{i,0}$ is the value of the dimensionless parameter at the present day for each component, the evolution of these components is shown in figure 1.4, in this special case we consider $\Omega_k = 0$, due to the value measured by the Planck is $\Omega_{k,0} = 0.0007 \pm 0.0019$ and it suggests a flat universe approximately [13].

Chapter 2

Dark Energy

In the early 20th century, Edwin Hubble reported one of the most important observations that would change our understanding of the cosmos. The Hooker telescope at Mount Wilson Observatory was used to measure the distance to Andromeda and other spiral nebulae; this showed that such nebulae are outside and far beyond the Milky Way. Shortly after that, by measuring the velocities of these galaxies and comparing them with their distances, he concluded that they were all moving away from each other. From these results, Hubble concluded that the universe was expanding. This chapter is about one of the proposals to explain this universe expansion, known as *dark energy*.

2.1 Observations

2.1.1 Cepheids

Because of their high luminosity compared to other stars, Cepheid variables are commonly used to calculate distances to objects beyond the Milky Way. These stars take their name from Delta Cephei, the first of this type discovered by John Goodricke in 1784, located in the constellation Cepheus.

Cepheid variable stars are distinguished by their remarkable luminosity and brightness variations in a regular pattern (see Figure 2.1). In 1912, astronomer Henrietta Leavitt made a crucial discovery while analyzing photographic plates: she observed that variable Cepheids in the Small Magellanic Cloud exhibited a relationship between their apparent brightness and the period of their luminous fluctuations. Although, at that time, the distance to the Magellanic Cloud was unknown, the Cepheids were assumed to be at approximately the same distance. Therefore, Leavitt established a systematic connection between the absolute luminosity of these stars and their period of oscillation: the brighter a Cepheid was, the longer its period of variation.

In 1923, Edwin Hubble and his team identified the presence of several Cepheid variable stars in the Andromeda Galaxy (M31). Using Henrietta Leavitt's calibration, Hubble could calculate the distance to M31 and thus prove that it was a separate galaxy. Until then, M31 was believed to be part of the Milky Way. After determining the distances to other galaxies using Cepheids, in 1929 Edwin Hubble discovered that the speed at which a galaxy moves away from us is proportional to its distance, this is *Hubble's law* and tells us that the farther a galaxy is from us, the faster it moves away; this law can be interpreted as the result of the expansion of the Universe.

2.2 Supernova and the expansion of the universe

In 1998, two teams of researchers, the *High-redshift Supernova Search Team* (HSST) led by Riess and the *Supernova Cosmology Project* (SCP) led by Perlmutter, made observations that changed our understanding of the universe forever by discovering that the expansion of the universe is accelerating.

The use of type Ia Supernova simplifies the determination of cosmological parameters since it

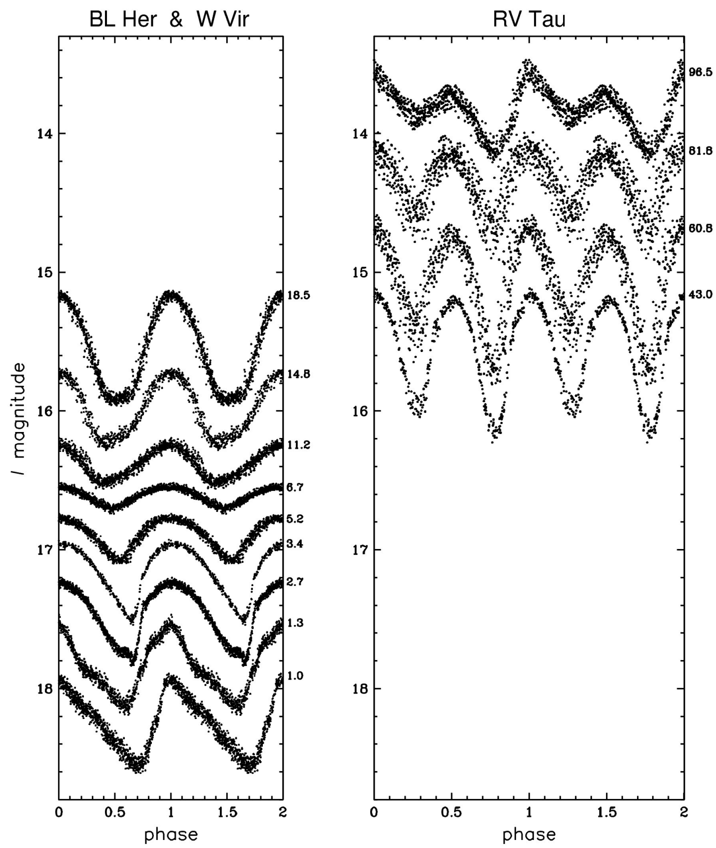

Figure 2.1: Example light curves of Type II Cepheids in the Large Magellanic Cloud (LMC). The left panel displays BL Her and W Vir stars, while the right panel features RV Tau stars, phased using their 'double' (formal) periods. The rounded periods of the light curves, in days, are indicated by small numbers on the right side of each pane [14]. Here, the phase represents a specific point in the star's repeating brightness cycle (its pulsation or variability cycle), while the magnitude is the brightness of the star at a specific point in its phase.

is possible to depict the entire method within a single graph. The fundamental concept revolves around identifying an object with a well-established brightness, often called a *standard candle* (stars with a known intrinsic luminosity), and mapping it to a Hubble diagram. This diagram illustrates the relationship between brightness (magnitude) and redshift (z) is shown in Figure 2.2 [15], where m is the apparent magnitude, i.e. this is how bright an object appears from the Earth, while M is the absolute magnitude M, this is how the bright the object would appear if it were placed at a distance of 10 parsecs, thus in this figure, $m - M$ is the modulus of distance and give us a way to calculate the distance to the object.

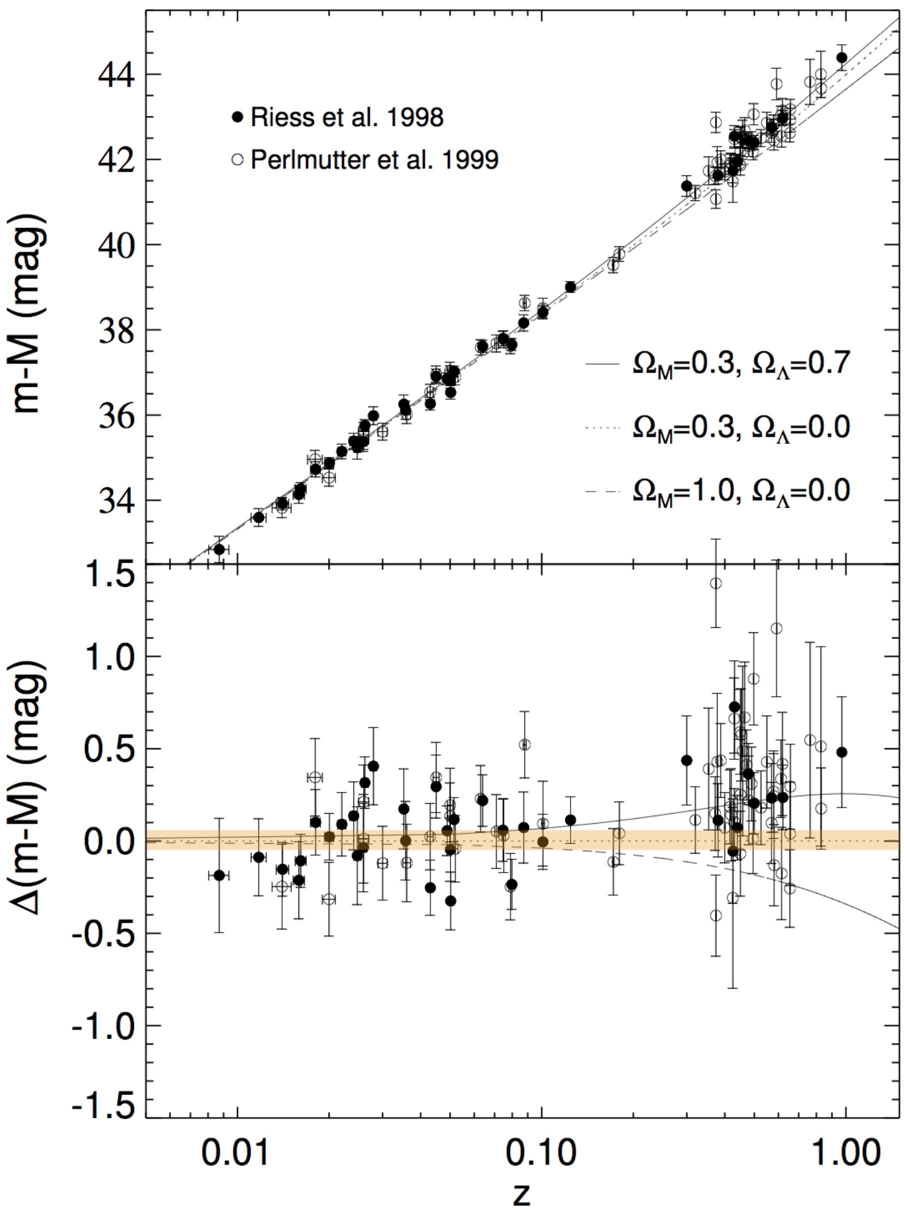

Figure 2.2: Type Ia supernova Hubble diagram, showing modulus of distance vs redshift [16]. The bottom panel shows residuals in distance modulus relative to an open universe with $\Omega_{m0} = 0.3$ and $\Omega_{\Lambda 0} = 0$

.

As shown in Figure 2.3 the confidence regions for the 42 supernovae set show that the universe's expansion will continue indefinitely, and the universe is accelerating, which is model-dependent. However, these findings do not provide insights into the universe's curvature. The elongated confidence region spans across the line, representing a flat universe, distinguishing between closed and open curvature.

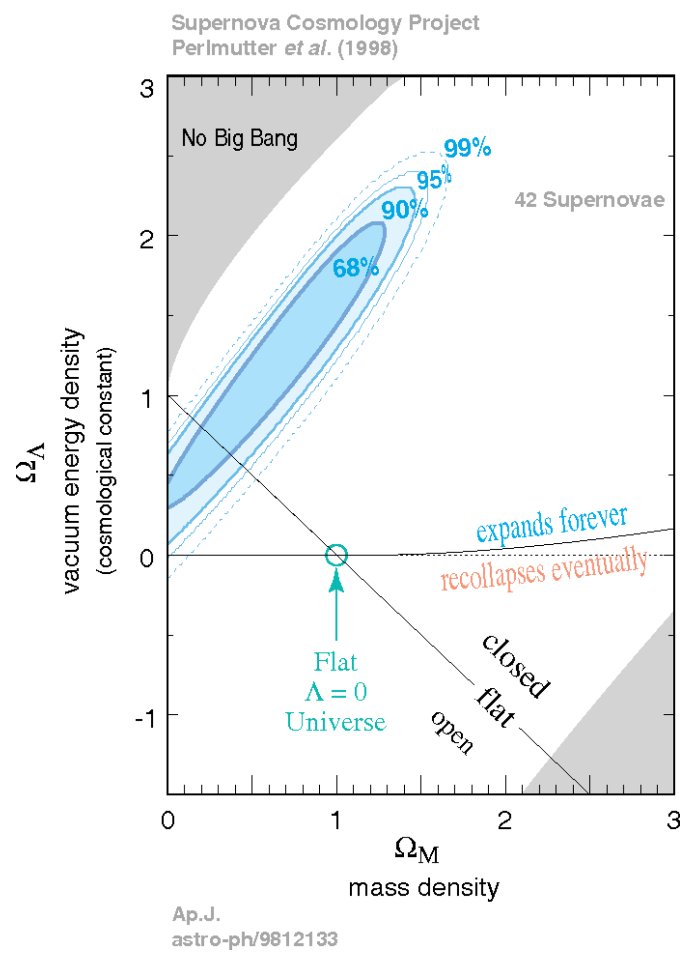

Figure 2.3: Confidence regions for matter and vacuum energy density, we consider only these two quantities because only these are relevant to the redshift associated with the observational data. [15].

Another significant inference drawn from the confidence region is that the data significantly deviate from the most straightforward cosmological model, which assumes flatness and zero cosmological constant. From these results, the universe's accelerated expansion is a fact; however, a new question, which to this day is one of the most important in cosmology, would arrive immediately: *what makes the universe expand in an accelerated way?* Again, one of the strongest candidates to explain this phenomenon is dark energy.

2.3 Cosmological Constant

In 1916, when Albert Einstein developed his general theory of relativity, the consensus of cosmology was that the universe was static, i.e., it did not expand. However, Einstein realized that his field equations describe a non-static universe. To reconcile his theory with this idea, introducing a new term into his equations was necessary to help counteract the effects of gravitational attraction. This new term introduced is known as the *cosmological constant* Λ. The new term is related to the *vacuum energy*, i.e. an energy density intrinsic to the empty space. For a long time, the cosmological constant term in Einstein's equations was forgotten, due to Hubble's observation of the expanding universe, however, from the observations of Riess and Perlmutter, the cosmological constant became relevant again, being the first candidate to explain the accelerated expansion of the universe.

With the cosmological constant term, the Einstein field equations are

$$R_{\mu\nu} - \frac{1}{2}\mathcal{R}g_{\mu\nu} + \Lambda g_{\mu\nu} = 8\pi G T_{\mu\nu}, \tag{2.1}$$

in the above equations, it has become common practice to shift this additional term to the right-hand side and regard it as part of the energy-momentum tensor $T_{\mu\nu} \longrightarrow T_{\mu\nu} + T^{(\Lambda)}_{\mu\nu}$, then we can define the quantity

$$T^{(\Lambda)}_{\mu\nu} = -\frac{\Lambda}{8\pi G}g_{\mu\nu} \equiv -\rho_\Lambda c^2 g_{\mu\nu} \tag{2.2}$$

we notice if compare this quantity with the energy-momentum tensor of the perfect fluid, given as [17]

$$T_{\mu\nu} = (\rho + p)u_\mu u_\nu + p g_{\mu\nu}, \tag{2.3}$$

the cosmological constant is like a perfect fluid with a negative pressure, in this case

$$p_\Lambda = -\rho_\Lambda.$$

This new term also has repercussions in Friedmann's equations, so these can be expressed as,

$$H^2 = \frac{8\pi G}{3}\rho + \frac{\Lambda}{3}, \tag{2.4}$$

$$\frac{\ddot{a}}{a} = -\frac{4\pi G}{3}(\rho + 3p) + \frac{\Lambda}{3}. \tag{2.5}$$

Due to the pressure of the cosmological constant is negative, work is done in the associated fluid as the universe expands, and then, this causes the density energy to remain constant even if the Universe's volume increases [8]. As we will see below, there is an important tension about the value of the energy density associated with the cosmological constant and with the value of energy density of the zero-point from QFT.

2.4 Cosmic distances

To understand the cosmological observations we will see below, it is necessary to introduce the cosmological distances involved. From the Friedmann-Lemaître-Robertson-Walker metric, we can rewrite the spatial part of the metric in a more practical way, for this, consider $d\chi \equiv dr/\sqrt{1 - kr^2/R_0^2}$, from this we can rewrite

$$ds^2 = dt^2 - a^2(t)\left[d\chi^2 + S^2(\chi)\left(d\theta^2 + \sin^2(\theta)d\phi^2\right)\right], \tag{2.6}$$

where the $S(\chi)$ is defined as

$$S(\chi) \equiv R_0 \begin{cases} \sin(\chi/R_0) & \text{if } k = +1, \\ \chi/R_0 & \text{if } k = 0, \\ \sinh(\chi/R_0) & \text{if } k = -1, \end{cases} \tag{2.7}$$

or it can be rewritten in the form

$$S_k(\chi) = \frac{1}{\sqrt{-k}} \sinh(\sqrt{-k}\chi),$$

considering the 3 different cases for k recovers each spatial curvature.

2.4.1 Comoving distance

Consider the case of light traveling in the direction of χ ($\theta = \phi =$ constant) the interval is

$$ds^2 = dt^2 - a^2(t)d\chi^2 = 0.$$

Now if we consider the case of a light beam emitted at time t_1 at the point χ_1, and this light beam this light beam arrives at an observer at time t_0 with $\chi = 0$. Thus, from this interval, we can define the *comoving distance* in the form

$$d_c \equiv \int_0^{\chi_1} d\chi = -\int_{t_0}^{t_1} \frac{dt}{a(t)}, \tag{2.8}$$

from the redshift's definition, we can express the comoving distance as

$$d_c = \frac{1}{a_0 H_0} \int_0^z \frac{dz'}{E(z')}, \tag{2.9}$$

where $E(z) = \frac{H(z)}{H_0}$.
Notice that, it is possible to carry out an expansion of (2.9) around $z = 0$, thus the integral takes the form

$$\int_0^z \frac{dz'}{E(z')} = z - \frac{E'(0)}{2} z^2 + \frac{1}{6} \left(2E'(0) - E''(0)\right) z^3 + O(z^4), \tag{2.10}$$

from this expansion notice that the limit case when $z \ll 1$, the comoving distance is approximately

$$d_c \approx \frac{z}{a_0 H_0}. \tag{2.11}$$

2.4.2 Luminous distance

In cosmology, the luminous distance is usually defined as

$$d_L^2 \equiv \frac{L_s}{4\pi F}, \tag{2.12}$$

where L_s is the magnitude of the luminosity of a source and F is the observed flow. Likewise, the flow is defined as $F = \frac{L_0}{S}$, with L_0 at $\chi = 0$ $(z = 0)$, also, the area of the sphere at $z = 0$ is $S = 4\pi(a_0 S_k(\chi))^2$.
Therefore, we can rewrite (2.12) in the form

$$d_L^2 = (a_0 S_k(\chi))^2 \frac{L_s}{L_0}. \tag{2.13}$$

On the other hand, notice that

$$\frac{L_s}{L_0} = \frac{\Delta E_1 \Delta t_0}{\Delta E_0 \Delta t_1} = (1+z)^2,$$

where ΔE_1 and Δt_1 is the energy emitted in a time interval. Therefore, the luminous distance takes the form

$$d_L = a_0 S_k(\chi)(1+z), \tag{2.14}$$

using the comoving distance (2.9), we get that the luminous distance is

$$d_L = \frac{c(1+z)}{H_0\sqrt{\Omega_{k,0}}} sinh\left(\sqrt{\Omega_{k,0}} \int_0^z \frac{dz'}{E(z')}\right). \tag{2.15}$$

From this result, we can now use the Taylor series in the form

$$sinh(x) = x + \frac{x^3}{6} + \mathcal{O}(x^5) \tag{2.16}$$

and using the equation (2.10), we find that around $z = 0$, the expression is

$$d_L \approx \frac{c}{H_0}\left[z + \left(1 - \frac{E'(0)}{2}\right) z^2 \frac{1}{6}\left(2E'(0)^2 - 3E'(0) - E''(0) + \Omega_{k,0}\right) z^3\right]. \tag{2.17}$$

2.4.3 Angular diameter distance

The angular diameter distance is defined as

$$d_A \equiv \frac{\Delta x}{\Delta \theta}, \tag{2.18}$$

If we consider that the source is located on the surface of a sphere of radius χ with an observer in the center with size Δx at t_1, we get

$$\Delta x = a(t_1) S_k(\chi) \Delta\theta, \tag{2.19}$$

thus, the diameter distance is

$$d_A = a(t_1) S_k(\chi) = \frac{a_0 S_k(\chi)}{1+z} = \frac{1}{1+z} \frac{c}{H_0 \sqrt{\Omega_{k,0}}} sinh \left(\sqrt{\Omega_{k,0}} \int_0^z \frac{dz'}{E(z')} \right), \tag{2.20}$$

comparing the above expression with (2.15), the relation is given by

$$d_A = \frac{d_L}{(1+z)^2}. \tag{2.21}$$

2.5 Cosmological tensions

In the current cosmology scenario, there are many inconsistencies or *cosmological tensions* concerning the standard cosmological model and the observations, many times people refer to these as Λ*CDM tensions*. Nevertheless, these inconsistencies are not specifics of this model, but these are limitations of the standard cosmological model and each solution to these tensions represents crucial knowledge about the universe. In this section, we study briefly some of these.

2.5.1 Old cosmological constant problem

One of the main discrepancies of the ΛCDM model arises when we want to compare the value of the energy density of the vacuum to the associated cosmological constant. The adjective ‘old’ is due to there being more problems associated with the cosmological constant, and this has remained since decades ago.

To notice this, we must be sure that the order of the cosmological constant is that of H_0^2, this is

$$\Lambda \approx H_0^2 = \left(2.133\, h \times 10^{-42}\, \mathrm{GeV}\right)^2, \tag{2.22}$$

with $h \approx 0.7$. Notice that we can consider an energy density associated, as follows,

$$\rho_\Lambda \sim \frac{\Lambda}{8\pi}\, m_{pl}^2 \sim 10^{-47}\, \mathrm{GeV}^4, \tag{2.23}$$

and where the Planck's mass is $m_{pl} \approx 10^{19}\, GeV$.

As Weinberg mentioned in [18], the energy density of the vacuum or the zero-point and the associated density energy to the cosmological constant are comparable, if we introduce the energy tensor of the point-zero energy in Einstein's field equation.

If we consider a flat space-time like Minkowski space-time, the only invariant tensor is $\eta_{\mu\nu}$, and since the vacuum state must be always the same for all observers [19], i.e. $\langle T_{\mu\nu}\rangle \propto \eta_{\mu\nu}$, if we extrapolate this in curved space-time, this means that

$$\langle T_{\mu\nu}\rangle = -\langle \rho_{\mathrm{vac}}(t, \vec{x})\rangle g_{\mu\nu}, \tag{2.24}$$

where is ρ_{vac} is the vacuum energy density. Now, using the fact that the energy-momentum tensor must be conserved, the ρ_{vac} must be constant, from this we can write

$$\langle T_{\mu\nu}\rangle = -\langle \rho_{\mathrm{vac}}\rangle g_{\mu\nu}. \tag{2.25}$$

The value of this energy density is calculated by summing the zero-point energies of all normal modes of some field of mass m up to a wave number cutoff $\Lambda \gg m$ (it is not the cosmological constant), yields a Vacuum energy density ($\hbar = c = 1$) [18]

$$\langle \rho_{\mathrm{vac}}\rangle = \int_0^\Lambda \frac{4\pi k^2 dk}{(2\pi)^3} \frac{\sqrt{k^2 + m^2}}{2} \simeq \frac{\Lambda^4}{16\pi^2}, \tag{2.26}$$

and considering the general relativity up to the Planck scale, the estimated value is

$$\langle \rho_{\text{vac}} \rangle \sim 10^{74}\,\text{GeV}^4. \tag{2.27}$$

From this, we can note the discrepancy between this estimated value and the observer value 2.22 is around 10^{121} times. Sometimes this discrepancy is interpreted as a kind of *fine-tuning problem,* due to it is necessary fine-tuning to reconcile both values.

2.5.2 The coincidence problem

This other problem within the ΛCDM framework is associated with the values of Ω_Λ and Ω_m, which are almost the same order of magnitude today. If we equal both density parameters and use Friedmann's constraint at present for a Universe dominated by matter and vacuum, it is possible to find the redshift-associated

$$z_{equality} = \left(\frac{\Omega_{\Lambda 0}}{1-\Omega_{\Lambda 0}}\right)^{1/3} - 1 \approx 0.3, \tag{2.28}$$

for the vacuum's density parameter at the present time $\Omega_{\Lambda,0} \approx 0.7$.
More specifically, during the universe's expansion, the density of matter decreases with time due to dilution caused by the increase in volume. In contrast, the density of dark energy remains relatively constant or even increases. This means that matter density was dominant over dark energy in earlier epochs. Still, in the present epoch, both densities are of the same order of magnitude, giving rise to why this is happening just now in cosmic history.
The coincidence problem raises questions about whether this situation is a chance occurrence, or whether some underlying principle or physical mechanism is explaining why these densities are comparable in the present epoch. Resolving this problem could offer a deeper understanding of the nature of dark energy and its relationship to the universe's evolution.

2.5.3 Hubble tension

The *Hubble tension* refers to the discrepancy of Hubble's parameter today, H_0 for local measurements and from the early universe. Remember, it represents the expansion rate of the universe measured today $z = 0$, thus its accuracy is fundamental due to many implications of its value, such as the age of the universe.

One of the most accurate measurements of H_0 from the early universe is by the cosmic microwave background (CMB) data. The nine-year *Wilkinson Microwave Anisotropy Probe* (WMAP) project informed the measure of H_0 using observations from CMB in 2013, the value in this case is $H_0 = 70.00 \pm 2.20$ km/s/Mpc, while, the *Planck* space observatory informed the value 67.40 ± 0.50 km/s/Mpc in Planck2013 results and also if other observational data is added to Planck results, this value is 67.36 ± 1.40 km/s/Mpc for Planck2018+lensing. Other predictions of H_0 by projects like the Atacama Cosmology Telescope (ACT) and South Pole Telescope (SPTPol) agree with the estimated value by Planck2018 result [20].

On the other hand, the estimated value by "local observations" such as Cepheid variables and SNe Ia is 72 ± 8km/s/Mpc using a modified distance calibration. One of the latest local values is given by SH0ES project, which is 73.04 ± 1.04 km/s/Mpc.

For the above reasons, there is a clear discrepancy between local observations and observations from the early universe, currently, many people are working from different perspectives to alleviate this obvious tension.

2.6 Beyond ΛCDM model

The above tensions on the ΛCDM model are the main motivation and justification for exploring possible extensions or modifications of this model, such as the introduction of new physics (e.g. dynamical dark energy or additional particle interactions) that in some way reproduces the ΛCDM model due to its great success with current observations. Usually, the extension of the ΛCDM model occurs using two types of modifications: the first is by introducing new degrees of freedom, which are represented by variables, i.e., modifying the cosmology, and the second way is by directly modifying the theory of gravity considered as the starting point, i.e., Einstein's theory of relativity by modifying the Einstein field equations or the Einstein-Hilbert action.
This section studies the most common extensions or alternatives to the Λ constant as the origin of the dark energy.

2.6.1 Parametrization

- **Lineal parametrization**: One of the simplest cases is to consider the EoS as a linear function around $z = 0$ [21], i.e.
$$\omega(z) = \omega_0 + \omega_1 z.$$

- **Chevallier-Polarski-Linder parametrization (CPL)**: This parameterization has some advantages compared to the previous parameterization, such as providing a reduction to the old linear redshift behavior for high redshift, high accuracy in the reconstruction of many scalar field equations of state and the resulting redshift-distance relationships, among others [22]
$$\omega(z) = \omega_0 + \frac{\omega_a z}{1+z}.$$

- **Barboza-Alcaniz parametrization (BA)**: This parameterization was proposed in 2008 by E. M. Barboza and J. S. Alcaniz, who proposed the parameterization of EoS in the following form [23]
$$\omega_{BA}(z) = \omega_0 + \omega_1 \frac{z(1+z)}{1+z^2}.$$

Even though the previous parameterizations had great success in each of the applied problems, they have a phenomenological basis, so that, because there are many observations, today we have a large catalog of different parameterizations. This creates a problem because only through a statistical analysis we can discard which of the parameterizations is better, which would take a long time, for this reason, we are interested in fundamental models that give us a parameter of the equation of state which is free of phenomenological arguments.

2.6.2 Scalar Field Models of Dark Energy

One of the most popular scalar fields to modulate the dark energy is known as *Quintessence*. This is a dynamic scalar field, in this way the equations of the state may vary over time, for example. The importance of this model lies in the possibility of linking the origin of the dark energy with the quantum field theory through the scalar fields [1].

[1] In this section consider the high-energy convention such as the interval is given by $ds^2 = -dt^2 + a(t)^2 d\vec{x}^2$.

In this frame, the quintessence is given by a canonical scalar field ϕ with the associated potential, $V(\phi)$ which interacts only gravitationally. The total action in this case is [24]

$$S = \int d^4x\sqrt{-g}\left[\frac{M_{pl}^2}{2}\mathcal{R} - \mathcal{L}\right] + S_m, \tag{2.29}$$

where $M_{pl}^{-1} = 8\pi G$ the Planck mass, S_m is the matter action, $\mathcal{R}$ the Ricci tensor and the Lagrangian

$$\mathcal{L} = -\frac{1}{2}g^{\mu\nu}\partial_\mu\phi\partial_\nu\phi - V(\phi), \tag{2.30}$$

Using this Lagrangian density, the energy density and the pressure in this model are given by $\rho_\phi = \frac{\dot{\phi}^2}{2} + V(\phi)$ and $p_\phi = \frac{\dot{\phi}^2}{2} - V(\phi)$, where the doc represents a derivative with respect to the cosmic time t. Thus the parameter of the equation of state is given by

$$\omega_\phi = \frac{\dot{\phi}^2 - 2V(\phi)}{\dot{\phi}^2 + 2V(\phi)}. \tag{2.31}$$

In the same way, we can find the associated continuity equation using the expression of the energy density and the parameter of Eo. This equation is

$$\ddot{\phi} + 3H\dot{\phi} + V_{,\phi} = 0, \tag{2.32}$$

where $V_{,\phi} = dV/d\phi$. This is the Klein-Gordon equation and describes the evolution of the scalar field. Notice that from (2.31), the slow roll limit is given by the $\dot{\phi}^2 << V(\phi)$ condition, as consequence, we obtain $\omega_\phi \approx -1$, which is the case of an accelerated expanded universe.
There are more models of dynamic dark energy based on scalar fields (the Lagrangian is different in each case) which include the $K - essence$ scalar field, the Phanthom scalar field, the quintom scalar field, and the scalar field model for the early dark energy case, as Axion-like Early Dark Energy (axEDE), Rock 'n' Roll Early Dark Energy ((RnR EDE)), Acoustic Early Dark Energy (ADE) [25] and others.

2.6.3 Interacting dark energy

This model considers the energy exchange through non-gravitational effects between dark energy and dark matter. This consideration becomes interesting if we remember that very close to us, the matter and dark energy quantities in the universe, are comparable. The exchange of energy is mediated by the *interaction factor* Q, this quantity is usually referred to just as *interaction*. The new factor is introduced in the cosmology model by modifying the continuity equations for the dark matter and dark energy, in the form [26]

$$\dot{\rho_{dm}} + 3H\rho_{dm} = Q, \tag{2.33}$$

$$\dot{\rho_{de}} + 3H(1+\omega)\rho_{de} = -Q. \tag{2.34}$$

Some of the common choices of this interaction parameter Q are [27]

- Assume the interaction is proportional to the dark matter density and the Hubble parameter, i.e. $Q \propto \rho_{dm}H$. It is the most simple approach and the most widely used one because it agrees with energy conservation in a flat universe.
- Another frequently used model combines both dark matter and dark energy densities $Q = H\left(\Gamma_a\rho_{dm} + \Gamma_b\rho_{de}\right)$, where, in this case, Γ_a and Γ_b are phenomenological constants. This choice for more flexible interactions that can help address cosmological tensions such as the Hubble tension.
- A general choice is given by considering different power indices for dark matter and dark energy densities $Q \propto \rho_{de}^n\rho_{dm}^m$. This case is useful for exploring complex scenarios.

Notice that the continuity equations for baryonic matter, radiation, or curvature, are not modified. Notice that from the modified continuity equation for the dark energy, the ω parameter is not specified, in this way, we can combine this model with another model with ω not constant. One important aspect of Q is the allowed sign, thus, the sign represents the convention of the energy transferred. For this reason, consider the following convention

1. If $Q < 0$, the energy is transferred from dark matter to dark energy.
2. If $Q > 0$, the energy is transferred from dark energy to dark matter.

3. If $Q = 0$, There isn't energy exchange between these sectors.

In this model, the choice of interaction parameter and the exchange density direction play a crucial role in solving some cosmological tension, such as the coincidence problem, Hubble tension, and the σ_8 as is explored in [26], [28] and [29].

2.6.4 Dark Energy Radiation

As mentioned above, the possibility of introducing a scalar field in dark energy models could give us a link between cosmology and high energy physics, however, it is necessary to take into account other essential factors due to the nature of both scenarios. Slowly rolling scalar fields are a minimalist model class that relates the properties of dark energy with particle physics, where traditionally the kinetic energy of the rolling scalar field constitutes the Dynamical part of dark energy. In this way, coupling scalar fields to light degrees of freedom, it is possible to modify this scenario by giving rise to the dissipation of the scalar field's energy into dark radiation, and it can constitute the dominant dynamical component of the dark energy as is explored in [30] for a minimal extension. In that work, the authors postulated the existence of a thermalized component of dark radiation, which slowly grows as the universe expands, and they named it *dark energy radiation* (DER).

To understand this model, consider a dynamical scalar field ϕ, initially displaced from its equilibrium value and slowly evolving towards it is often invoked to model dark energy and considering the particle production due to the coupling Π_{int} to a light sector, then, for a dynamical scalar field ϕ, and in this particular case, we can write the Lagrangian as $\mathcal{L} = -\phi\Pi_{int}$. The direct consequence of this idea is the possibility of modifying the dynamics and, then, the cosmological observable parameters associated with the dark energy.
The particle production could result from various quantum phenomena, in the case of the production given by thermal friction. The energy density will characterized by the associated temperature, in the form [31]

$$\rho_{de} = \frac{\pi^2 g_*}{30} T_{\mathrm{DER}}^4, \tag{2.35}$$

where g_* are the degrees of freedom in the light sector. Some models have shown the linear and cubic temperature dependencies of the friction coefficients [32], thus, we can summarize these cases in the following definition

$$\Gamma(\rho_{\rm DER}) \equiv c_n \rho_{DER}^{n/4}, \quad n = 0 \text{ or } 3, \tag{2.36}$$

this thermal friction term could have two interesting implications in the evolution of the scalar field and its accompanying dark radiation. First, for the linear friction case, the time-evolution of the scalar field is modified, and second, the scalar field sources dark radiation that doesn't redshift as respected for radiation it gets replenished by the scalar field [33]. The dynamics of the scalar field, in this case, is given by the following coupled

$$\ddot{\phi} \; + \; (3H + \Gamma)\dot{\phi} + \frac{dV(\phi)}{d\phi} = 0, \tag{2.37}$$

$$\dot{\rho}_{\rm DER} + 4H\rho_{\rm DER} = \Gamma\dot{\phi}^2, \tag{2.38}$$

with $V(\phi)$ as the associated potential to the scalar field. Notice the limit when $V(\phi) \gg \rho_{DER}$, $\dot{\phi}^2$, the sum of the scalar field and dark radiation energy densities is compatible with the observed properties of dark energy.

Similarly to the above models, there are different scenarios or submodels, in this case, we can characterize all of them from the friction coefficient. The first case is known as the *minimal dark energy radiation*, and it is the case for $n = 3$, thus, friction factor is $\Gamma = c_3\rho_{\rm DER}^{3/4}$. Furthermore, for the agreement with the dark energy behavior, the scalar field needs to evolve slowly, and the potential should be in the form $V(\phi) = -C\phi$. There are other sub-scenarios, which include a friction coefficient constant, the possibility of using the Quintessence scalar field, or some parametrization as mentioned at the beginning of this chapter.

Chapter 3

Holographic Dark Energy

To better understand the holographic dark energy model, it is necessary to understand the ideas related to the holographic principle and the Bekenstein-Hawking formula for black hole entropy. For this reason, reviewing chapter 4 about the holographic principle from *M-Theory and Quantum Geometry* book [34] is recommended.

In this chapter, we will review the holographic dark energy model, starting from the Bekenstein-Hawking formula and the quantum field theory estimates for the vacuum energy density. In addition, generalizations of this model using entropies associated with different physical systems and generalizations of the exponent in the Barrow model.

3.1 Standard holographic dark energy model

The holographic dark energy model is one of the many applications of the *holographic principle* to solve the problem of dark energy in cosmology. This principle was proposed by Gerard't Hooft in 1993 when he studied black hole thermodynamics, and it establishes that *all information in a volume of space can be described by the boundary of that space*, following the hologram's idea. This idea has greatly succeeded in high-energy physics, particularly the works by Juan Maldacena and Leonard Susskind.

Keeping this line of thought, Bekenstein considers a box of size L with UV cut-off Λ_c in effective field theory and applying the analogy from black hole thermodynamics, he postulated that the maximum entropy behaves nonextensive, growing only as the area of the box. This is the Bekenstein entropy bound given by

$$S \leq S_{BH} \equiv \pi M_p^2 L^2. \tag{3.1}$$

However, this nonextensive scaling implies that quantum field theory fails in large volumes. Consequently, Cohen, Kaplan, and Nelson in 1999 [35] reconcile this issue with the success of local quantum field theory in explaining observed particle behavior, by proposing a more constraining bound, they considered that in the quantum field theory, a short distance (UV) cut-off is associated to a long-distance (IR) cut-off due to the limit set by forming a black hole. In this way, if the quantum zero-point energy density ρ_{de} is relevant at some UV cut-off, the total energy of the whole system with size L should not exceed the mass of a black hole of the same size, and using the fact that Λ^4 is the maximum energy density in the effective theory, this new constrain is given by

$$L^3\Lambda^4 \lesssim L M_p^2. \tag{3.2}$$

On the other hand, Miao Li considers (by a dimensional analysis) a general expression of the dark energy density for a universe with a characteristic length scale L, it only depends on M_p and the cosmological length scale L, thus [36]

$$\rho_{\rm de} = \alpha_1 M_{pl}^4 + \alpha_2 M_p^2 L^{-2} + \alpha_3 L^{-4} + \ldots \tag{3.3}$$

where each α is a constant. Notice that, the first term has the same form of the vacuum energy density of the fine-tuning problem and also if we compare the above expression to the result by Cohen et al. the first term is not compatible with the holographic principle due to $\rho_{de} \sim \alpha_1 M_{pl}^4$ is the traditional estimation from local quantum field theory and as Cohen et al. have stressed, the local quantum field theory should not be a good description for a black hole or states at the scale of its Schwarzschild radius. It is important due to the energy within a Schwarzschild l is given by $l^3\Lambda^4$ and it should be less than the mass of a corresponding black hole, thus, we can despise the first term.

One result from (3.2) is that the zero-point fluctuation estimated from this UV cut-off is given by

$$\rho_{de} \sim \Lambda^4 \lesssim L M_{pl}^2, \tag{3.4}$$

For these reasons, Miao argues that only the second term in 3.3 is relevant (the rest of the terms have lower scales), and then, for the largest allowed value of L, the equality is satisfied as follows

$$\rho_{\rm de} = 3c^2 M_p^2 L^{-2}, \tag{3.5}$$

with c a new constant parameter. An alternative expression to (3.2) can be found if we remember that the Bekenstein-Hawking formula for the entropy of a black hole $S_{BH} \propto M_{pl} L^2$, the constraint can be expressed as

$$\rho_{de} \lesssim L^{-2} S_{BH}. \tag{3.6}$$

3.1.1 Future event horizon as the characteristic length scale

If the maximum allowed value of L, can be taken as the current size, i.e., at the Hubble scale ($L = H^{-1}$), it is possible to consider this energy density as the one associated with dark energy at present. If one considers a Universe that is dominated only by dark energy and matter, the associated Friedmann equation in Planck units can be expressed, as

$$3M_p^2 H^2 = \rho_m + \rho_{de}. \tag{3.7}$$

Hsu showed in 2004 that this choice on the scale of L is incorrect because the resulting equation of state for dark energy is $\omega_{de} = 0$ [37]. Based on this result, Hsu points out there is the possibility that entropy bounds may only apply to Λ on a cosmological scale. Thus, there is no apparent reason why the concept of holography couldn't be extended to smaller systems within our universe. Nevertheless, Miao Li solved in 2004 this problem about the choice of the horizon using a new horizon by a shrinking Hubble scale [38]. This is the future event horizon given by

$$R_h = a \int_t^\infty \frac{dt'}{a(t'x)} = a \int_a^\infty \frac{da'}{Ha'^2}, \tag{3.8}$$

this new horizon can be interpreted as the boundary of some volume for a fixed observer may eventually observe.

To find a general expression for the evolution of holographic dark energy, consider the derivative respect to cosmic time of the dark energy density parameter and use its respective conservation equation, then we get

$$\dot{\Omega}_{de} = -3H\Omega_{de} - 3H\Omega_{de}\frac{P_{de}}{\rho_{de}} - 2\Omega_{de}\frac{\dot{H}}{H}\,, \tag{3.9}$$

now, consider deriving the Hubble equation 3.7 with respect to cosmic time

$$2H\dot{H} = \frac{8\pi G}{3}\dot{\rho}_{tot}\,, \tag{3.10}$$

replacing the conservation equations and isolating the DE pressure:

$$\frac{\dot{H}}{H^2} = -\frac{4\pi G}{H^2}\left(\rho_m + P_{de} + \rho_{de}\right)\,, \tag{3.11}$$

or,

$$\frac{\dot{H}}{H^2} = -\frac{3}{2}\left(\Omega_m + \Omega_{de}\right) - \frac{4\pi G}{H^2}P_{de}\,, \tag{3.12}$$

then identifying the Friedmann constrain $\Omega_m + \Omega_{de} = 1$, and using the definition of the critic density, we get the following expression for the dark energy pressure

$$P_{de} = -\frac{\dot{H}}{H^2}\frac{2}{3}\rho_{crit} - \rho_{crit}\,. \tag{3.13}$$

Finally, replacing this expression in 3.9, we get the general differential equation for the holographic dark energy density parameter

$$\dot{\Omega}_{de} = 2\frac{\dot{H}}{H}(1-\Omega_{de}) + 3H\left(1-\Omega_{de}\right), \tag{3.14}$$

now if we use the future event horizon as the scale $L = R_h^{-1}$, from (3.5), one can get

$$\int_a^{\infty} \frac{da'}{Ha'^2} = \frac{c}{aH\sqrt{\Omega_{de}}}. \tag{3.15}$$

taking the derivative in the last expression and using the fundamental theorem of calculus, the evolution of the Hubble parameter is

$$\frac{\dot{H}}{H} = \frac{H\sqrt{\Omega_{de}}}{c} - H - \frac{\dot{\Omega}_{de}}{2\Omega_{de}}. \tag{3.16}$$

Notice that, replacing this expression in the equation (3.14), the differential equation as a function of the redshift, is

$$\boxed{\frac{1}{\Omega_{de}}\frac{d\Omega_{de}}{dz} = \frac{\Omega_{de}-1}{z+1}\left(1+\frac{2\sqrt{\Omega_{de}}}{c}\right)} \tag{3.17}$$

From this, we can see that $0 < \Omega_{de} < 1$, thus the evolution of the dark energy density parameter is always negative, and in precision, this always increases in the future ($z \longrightarrow -1$).

The EoS parameter can be found using the derivative of density energy (3.5) again and the conservation equation of the dark energy. This parameter is given by

$$\boxed{\omega_{de} = -\frac{1}{3}\left(1+\frac{2\sqrt{\Omega_{de}}}{c}\right).} \tag{3.18}$$

In the case of a universe dominated only by dark energy ($\Omega_{de} = 1$), the above parameter reproduces the ΛCDM case. Also, as you can see, this parameter only depends on the solution of the differential equation of the Ω_{de}.

Now we can solve the above differential equations and various values of the parameters in each model using the `odeint` method in Python, and using these solutions we can plot the Hubble parameter for different values of c, then in this way we can compare with the data points of $H(z)$. In addition, this is useful for later defining our parameter priors in each model.

Furthermore, notice that for plot the $H(z)$, the dark energy density can be expressed as $\rho_{de} = \Omega_{de}\rho_c = \Omega_{de} 3H^2 M_p^2$, thus from the Friedmann equation, we get

$$H(z) = H_0 \left(\frac{\Omega_{m,0}(1+z)^3}{1-\Omega_{de}(z)} \right)^{1/2} . \tag{3.19}$$

This is a general equation for the Hubble parameter, in this case, the dark energy parameter density $\Omega_{de}(z)$, is the solution of the differential equation for the holographic model. The solutions of the equation (3.17) and $H(z)$ for different values of the c parameter are shown in figure 3.1, as you can see there are some values of c are further away from the data points than others, thus, we consider exploring the region $0.5 \leq c \leq 1.5$ in the parameter space.

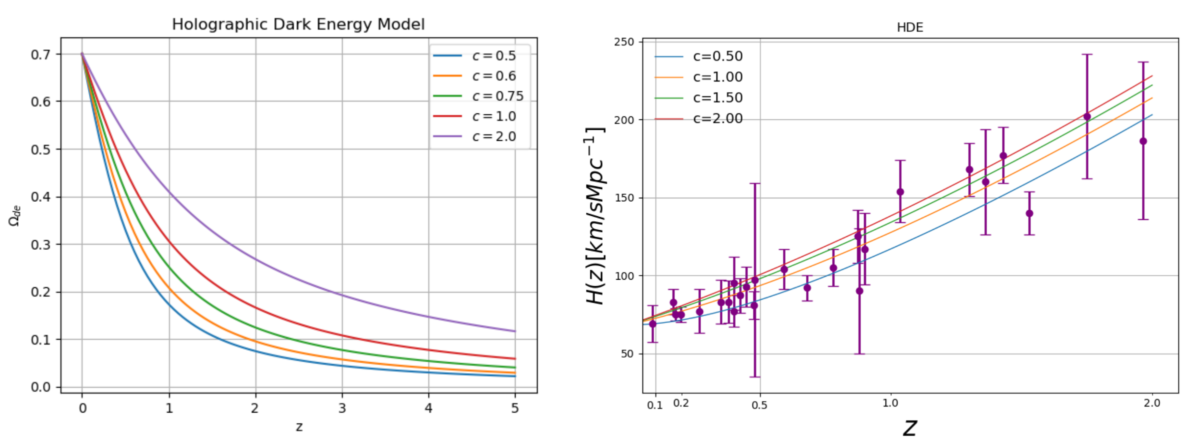

(a)

(b)

Figure 3.1: **(a)** Dark Energy density for the holographic dark energy model. **(b)** The variation of $H(z)$ with redshift z, in units when $M_p^2 = 1$ and $H_0 = 70\,\mathrm{km/s/Mpc}$. To be consistent with data, we use the initial condition $\Omega_{de}(z=0) = 0.7$. The bars represent the 26 $H(z)$ data points.

For this case, we solve the differential equation on an observational regime (from $z = 0$ to $z = 2$), nevertheless, the evolution of the holographic dark energy in the future ($z < 0$) has been studied by Eoin Ó Colgáin et al. in [39], where they analyzed the future scenarios and comment the possibility of a turning point in the Hubble diagram $H(z)$ at z_* i.e. $H'(z_*) = 0$. They found that the turning point depends on the c value, particularly $c < 1$, which is necessary to get this point in the future.

3.2 Beyond standard holographic dark energy

Due to the holographic dark energy depends entirely on entropy, we can use entropy expressions from more general systems. In the following sections, we refer to the above holographic dark energy model as the standard holographic dark energy model, and we will study the extensions to this model.

3.2.1 Holographic dark energy with spatial curvature

Many times building a dark energy model, usually we consider a flat universe, i.e., $k = 0$, and it is due to ΛCDM and inflation models, that the spatial curvature is very small and negligible, therefore. However, a dynamical dark energy's existence for a general case is necessary to consider a non-flat spatial curvature. From the definition of the future event horizon for a non-flat space case, we get [40]

$$\int_0^{r(t)} \frac{dr}{\sqrt{1-kr^2}} = \int_t^{\infty} \frac{dt}{a} = \frac{R_h}{a}, \tag{3.20}$$

in this case, the evolution of the dark energy parameter can be expressed as

$$\boxed{\frac{\Omega'_{de}}{\Omega^2_{de}} = \left(\frac{1}{\Omega_{de}\left(1 + a\Omega_{k,0}/\Omega_{de,0}\right)} + \frac{2}{c\sqrt{\Omega_{de}}} \cos \frac{\sqrt{k}R_h}{a} \right),} \tag{3.21}$$

considering the Friedmann constrain $\Omega_k + \Omega_{de} + \Omega_m + \Omega_r = 1$. As in the standard holographic dark energy model, when $c \sim 1$, the energy density of the dark energy will be constant. Notice that, the k constant can take negative values, as is the case of the open universe, thus, it is necessary to replace $\sqrt{k}$ with $\sqrt{|k|}$. The viability of this model has been explored using data from Supernovas and Cosmic Microwave Background. For the case of a closed universe, the favored values are $\Omega_{k,0} = -0.35^{+0.38}_{-0.17}$ and $c = 1.0^{+0.1}_{-0.17}$ using supernova data only, and using both data sets, the favored values are $\Omega_{k,0} = -0.02 \pm 0.1$, $c = 0.84^{+0.16}_{-0.03}$ [41]. For a non-constant spatial curvature, the equation of the state is the same, but, notice that Ω_{de} evolves differently in this case.

3.2.2 Time-Varying gravitational constant in holographic dark energy

Since the last century, the study of a varying gravitational constant has been carried out in the modified gravity models as a generalization of Newton's gravitational theory, this consideration could be applied to holographic dark energy in [42]. For a "gravitational constant" with time variation, the evolution of the dark energy density is,

$$\boxed{\frac{\Omega'_{de}}{\Omega_{de}(1-\Omega_{de})} = 1 + \frac{2\sqrt{\Omega_{de}}}{c} - \frac{G'}{G}(1-\Omega_{de})\Omega_{de}.} \tag{3.22}$$

Notice that the solution of this equation depends on the explicit form of G. From astrophysical observations, the constraint of Newton's constant is [43]

$$4.10 \times 10^{-11} yr^{-1} \leq \left|\frac{\dot{G}}{G}\right|, \tag{3.23}$$

there is another constrain from the Big Bang nucleo-synthesis theory, which is [44]

$$-3.0^{-13} \leq \frac{\dot{G}}{G} \leq 10^{-13} yr^{-1}. \tag{3.24}$$

This model has been tested with data from Supernovas, Cosmic Microwave Background, and baryon acoustic oscillation the values of the cosmological parameters are: $c = 0.8^{+0.16}_{-0.13}$ and $G'/G = -0.0025^{+0.0080}_{-0.0050}$ 1σ (here the $'$ represents the derivate respect $\ln a$) at confidence level [42].

3.2.3 Interacting holographic dark energy

As mentioned above, the possibility of interaction between dark energy and dark matter has been studied in different scenarios, the holographic dark energy is not the exception. In the general cases of a non-flat universe, the interaction is given by the parameter Q and it's introduced in the continuity equation of dark energy and dark matter in the same way of the subsection 2.6.3, where we mentioned the most common form of the interaction factor, nevertheless, there are multiple alternatives based on phenomenology as the following cases [36]

$$Q = \frac{H\rho_{dm}^{\zeta_1}\rho_{de}^{\zeta_2}}{\rho_c^{\zeta_1+\zeta_2-1}}, \tag{3.25}$$

$$Q = H\frac{\Gamma\rho_{de}\rho_{dm}}{\rho_{de}+\rho_{de}}, \tag{3.26}$$

$$Q = \Gamma\left(\dot{\rho}_{de}+\dot{\rho}_{dm}\right). \tag{3.27}$$

With the interaction and spatial curvature terms, the evolution of the holographic dark energy is given by

$$\frac{d\Omega_{de}}{dz} = -\frac{2\Omega_{de}(1-\Omega)}{1+z}\left(\sqrt{\frac{\Omega_{de}}{c^2}+\Omega_k}+\frac{1}{2}-\frac{\Omega_k-\Omega_r+\Omega_I}{2(1-\Omega_{de})}\right), \tag{3.28}$$

where $\Omega_I \equiv \frac{Q}{H(z)\rho_c}$. In the case of a flat universe, the EoS parameter is

$$\omega_{de} = -\frac{\Omega_{de}^{'}}{3\Omega_{de}(1-\Omega_{de})} - \frac{Q}{3H(1-\Omega_{de})\rho_{de}}. \tag{3.29}$$

The possibility to modulate the energy exchange of dark energy and dark matter in the holographic dark energy scenarios. Furthermore, the alleviation of the coincidence problem is impossible in the standard version of the holographic dark energy, because we need a constant horizon and this is not the case for the event's future horizon, thus, it is necessary to explore more generalized models of holographic dark energy. Furthermore, only about holographic dark energy, we can find many different approaches so far, extending the standard holographic dark energy model by incorporating other cosmological scenarios such as neutrino's physics in holographic dark energy model [45], considering that the fluctuations arise from the fluctuations in the size of the future event horizon [46], inflation [47], Brans-Dicke theory [48], scalar fields [49], [50] and other scenarios. In this work, we study the generalized exponents approach in holographic dark energy as a consequence of considering generalized entropies.

3.3 Entropy models in holographic dark energy

As we saw earlier, it is possible to describe the entropy of a black hole in a well-defined way. However, as usual in physics, adding new parameters to the already known quantities is often necessary to make a more complete system description. This is why many entropy models have been proposed to describe systems like black holes better and, as expected, always in some limit, reproduce the already known Bekenstein-Hawking formula. The properties that we expect generalized versions of the entropies have been [51]

- **Bekenstein-Hawking limit:**
  All the above entropies reduce to the Bekenstein-Hawking entropy S_{BH} in an appropriate limit.

- **Monotonically increasing functions:**
  All the above entropies are monotonically increasing functions of the S_{BH}.

- **Positivity:**
  All the above entropies are positive, as is the Bekenstein-Hawking entropy.

- **Generalized third law:**
  In the third law of standard thermodynamics for closed systems in thermodynamic equilibrium, the quantity $e^{S_{BH}}$ expresses the number of states or the volume of these states, and therefore the entropy vanishes when the temperature does because the ground (vacuum) state should be unique. By contrast, the Bekenstein-Hawking entropy diverges when the temperature T vanishes, and it goes to zero at infinite temperature. However, requiring any generalized entropy to vanish when the Bekenstein-Hawking entropy vanishes could be a natural requirement.

As we will see, the following generalized entropy alternatives share these characteristics.

3.4 Barrow holographic dark energy model

This model arose from the ideas of John D. Barrow in 2020 when he showed that the quantum-gravitational effects may introduce intricate fractal features on the black-hole structure [52].

Barrow proposed to model the horizon surface of a black hole as a fractal horizon surface. This fractal is constructed by joining several small spheres so that they touch their outer surface, with even smaller spheres touching the surfaces of those spheres, and so on consecutively. In this way, the most general case is when the surface of the black hole is only the fractal surface, the surface varies as $R^{2+\mathcal{B}}$ with the constrain $0 \leq \mathcal{B} \leq 1$. Notice the case when $\mathcal{B} = 0$, is the simplest horizon structure and the case $\mathcal{B} = 1$ is associated from an information perspective as if it possessed one geometric dimension higher [53].For this reason, Barrow's entropy is usually expressed as

$$\boxed{S_{\mathrm{B}} = \left(\frac{A}{A_p}\right)^{1+\mathcal{B}/2}}, \tag{3.30}$$

From the above definition of entropy, as in the case of the Bekenstein-Hawking entropy, it is possible to find expressions for the dark energy density using (3.6) and generalizing $S_{BH} \rightarrow S_{\mathrm{B}}$, we get for the case of the Barrow entropy

$$\rho_{\mathrm{B}} = 3c^2 M_p^2 L^{2-\mathcal{B}}. \tag{3.31}$$

Likewise, similarly in the standard holographic dark energy, in the Barrow's frame, we get the expression

$$\int_x^{\infty} \frac{da}{Ha^2} = \frac{1}{a}\left(\frac{N}{3M_P^2 H^2 \Omega_{de}}\right)^{\frac{1}{2-\mathcal{B}}}, \tag{3.32}$$

Notice that for the Universe dominated by matter and dark energy, the Friedmann constrain, we can rewrite

$$\frac{1}{Ha^2} = \frac{\sqrt{(1-\Omega_{DE})}}{H_0\sqrt{a\Omega_{m0}}},$$

replacing this expression in the horizon (3.32)

$$\int_{x}^{\infty}\sqrt{\frac{1-\Omega_{DE}}{a\Omega_{m0}}}\frac{da}{H_0}=\frac{1}{a}\left(\frac{N}{3M_p^2H^2\Omega_{DE}}\right)^{\frac{1}{2-\mathcal{B}}}. \tag{3.33}$$

Now differentiating this expression on both sides with respect to a, using the fundamental theorem of calculus and the variable change $x = ln(a)$, the differential equation for the evolution of the Barrow holographic dark energy is

$$\boxed{\frac{\Omega'_{de}}{\Omega_{de}\left(1-\Omega_{de}\right)}=1+\mathcal{B}+Q_{\mathcal{B}}\left(1-\Omega_{DE}\right)^{\frac{\mathcal{B}}{2(\mathcal{B}-2)}}\Omega_{DE}^{\frac{1}{2-\mathcal{B}}}e^{\frac{3\mathcal{B}}{2(\mathcal{B}-2)}x},} \tag{3.34}$$

where

$$Q_{\mathcal{B}}=(2-\mathcal{B})\left(\frac{N}{3M_p^2}\right)^{\frac{1}{\mathcal{B}-2}}\left(H_0\sqrt{\Omega_{m0}}\right)^{\frac{\mathcal{B}}{2-\mathcal{B}}}. \tag{3.35}$$

and with $N = 3M_p^2c^2$. By performing a procedure analogous to the one in the previous model, we get the EoS parameter

$$\omega_{de}=-\frac{1+\mathcal{B}}{3}-\frac{Q_{\mathcal{B}}}{3}\left(\Omega_{de}\right)^{\frac{1}{2-\mathcal{B}}}\left(1-\Omega_{de}\right)^{\frac{\mathcal{B}}{2(\mathcal{B}-2)}}e^{\frac{3\mathcal{B}}{2(2-\mathcal{B})}x}. \tag{3.36}$$

As we said earlier when we introduced Barrow's entropy, we recovered the standard holographic dark energy model on the limit $\mathcal{B} \longrightarrow 0$, thus, from the equation (3.34), it leads to

$$\frac{\Omega'_{de}}{\Omega_{de}(1-\Omega_{de})}=1+\frac{2\sqrt{\Omega_{de}}}{c}, \tag{3.37}$$

this is the differential equation for the standard holographic dark energy.
Notice that from figure 3.2 we can see that the value $\mathcal{B} = 1.9$ is far from the region of the other solutions, thus, we can discard for $\mathcal{B} < 2.0$ values. In addition, notice that the values in the region $0.5 \leq \mathcal{B} \leq 1.5$, look like the best fit to the data points, so it is ideal to explore this area during parameter inference, for the case of $\mathcal{B}$. In particular, we can see that for $c = 1.0$ looks like the best fit among all the solutions, of course, when we realize the inference of the parameter, the value of

c will be different.

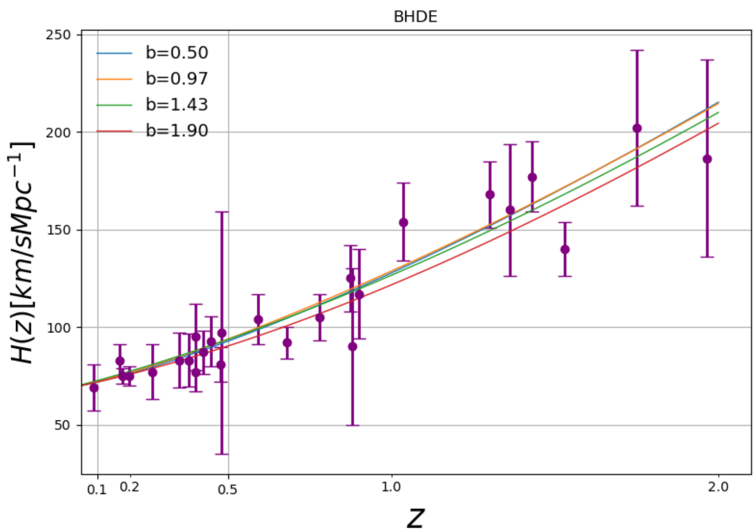

Figure 3.2: The Hubble factor $H(z)$ with redshift z, in units when $M_p^2 = 1$ and $H_0 = 70$. To be consistent with data, we use the initial condition $\Omega_{de}(z = 0) = 0.7\,\mathrm{km/s/Mpc}$.. The bars represent the 26 $H(z)$ data points.

3.4.1 About the second law of thermodynamics in the Barrow scenarios

Previously in Section 3.3, we have mentioned some properties of the cosmological models, which consider generalizations of the Bekenstein-Hawking entropy, however, an important aspect of these generalized models is the validity of the generalized second law of thermodynamics. In this section, we briefly review the application of the Barrow entropy and the implications in the associated generalized second law to understand the importance of its validity.

Saridakis et al. have pointed out this in [54] using the Barrow entropy and considering the total entropy as a sum of entropy enclosed by the apparent horizon and the entropy of the horizon itself (since as the horizon varies as the accelerated expansion of the universe), i.e. $S_{\text{total}} = S_{\text{de}} + S_{\text{m}} + S_{\text{h}}$.

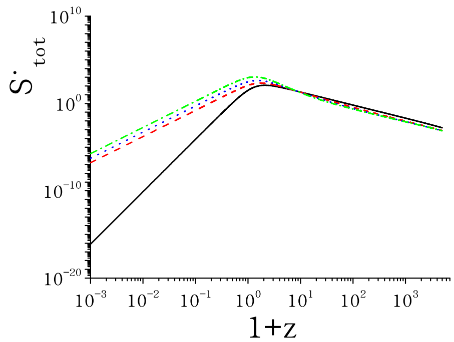

(a)

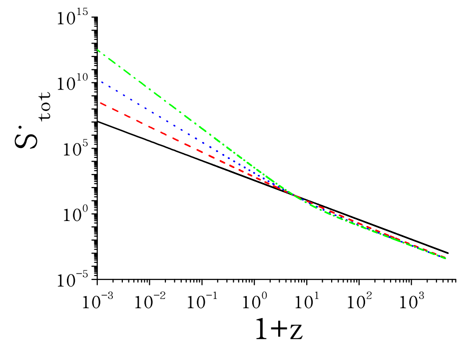

(b)

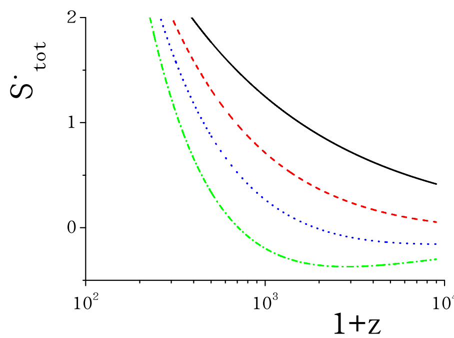

(c)

Figure 3.3: **(a)** The evolution of the entropy time-variation as a function of z for ΛCDM case. Black-solid line represents the value $\mathcal{B} = 0$,red-dashed line represents $\mathcal{B} = 0.3$, blue-dotted line represents $\mathcal{B} = 0.6$ and green-dashed-dotted represents $\mathcal{B} = 1.0$. **(b)** The evolution of the entropy time-variation as a function of z for the power-law background case, the order of the lines is the same as in the before case with $n = 2/3$ for all cases. **(c)** The evolution of the entropy time-variation as a function of z for the power-law background case, the order of the lines is the same as in the before cases but with $n = 2$ for all cases [54]. They imposed $c = H_0 = 1$.

They show that when the associated entropy to the horizon is the Barrow entropy, for the case $\mathcal{B} = 0$ (Bekenstein-Hawking limit) the total entropy is always a non-decreasing function of time, however, for the case $\mathcal{B} \neq 0$ the quantum-gravitational corrections switch on this is not true anymore, as is shown in figure 3.3. Thus, the generalized second law of thermodynamics can be conditionally violated depending on the evolution of the universe. First, they analyzed the case ΛCDM background cosmological evolution, they found that the entropy time-variation is always positive, and thus the generalized second law of thermodynamics is always valid. Nevertheless, in the case of a general power-law cosmological evolution like $H_{\text{power}} = H_0(1+z)^{1/n}$ with $H_0 = na_1^{1/n}$, for power-law exponents larger than one and suitably large $\mathcal{B}$ values, the entropy variation over time can be negative in the past, leading to a violation of the generalized second law. This highlights the importance of examining the generalized second law of thermodynamics in a generalized model.

Note that the second generalized law studied in that work is about the horizon and not for the background cosmology, as we intend to do in this work.

3.5 Tsallis holographic dark energy model

Tsallis entropy, named after Constantino Tsallis, who introduced it in the 1980s, is a generalization of the classical Boltzmann-Gibbs entropy commonly used in statistical mechanics. Unlike the Boltzmann-Gibbs entropy, which is based on the logarithmic function, Tsallis entropy is based on a $q - logarithmic$ function, where $q \in \mathbb{R}$ is a parameter that characterizes the deviation from the classical case [55].

Using the multifractal concepts and the probability p_i^q associated with an event, Tsallis postulated its entropy to generalize the standard expression of the entropy S in the information theory

$$S = -k\sum_{i=1}^{W} p_i ln(p_i),\ \forall\ W \in \mathbb{N}. \tag{3.38}$$

where W represents the total number of possible configurations. The generalized version by Tsallis is

$$S_q = k\frac{1-\sum_{i=1}^{W} p_i^q}{q-1}, \tag{3.39}$$

with k a conventional and $\sum_{i=0}^{W} p_i = 1$.

In 1902, Gibbs highlighted a limitation of the Boltzmann-Gibbs theory, noting its inapplicability to systems with divergent partition functions. We now understand that gravitational systems fall into this category. Tsallis later demonstrated that in such instances, the conventional Boltzmann-

Gibbs additive entropy, grounded in the assumption of weak probabilistic correlations and their association with ergodicity, requires generalization. This leads to the concept of non-additive entropy, where the entropy of the entire system may not necessarily equal the sum of the entropies of its subsystems, this is the case of the Tsallis entropy [56]. For the case of a black hole, the Tsallis entropy can be expressed as

$$\boxed{S_{\mathcal{T}} = \frac{A_0}{4G}\left(\frac{A}{A_0}\right)^{\delta}}, \tag{3.40}$$

with A_0 is area constant and δ is a dimensionless parameter. Notice that for $\delta = 1$ the Bekenstein-Hawking entropy is recovered.

From the above definitions of entropy, as in the case of the Bekenstein-Hawking entropy, it is possible to find expressions for the dark energy density using the equation (3.5), we get for the case of the Tsallis entropy

$$\rho_T = \mathcal{K} L^{2\delta - 4}, \tag{3.41}$$

where $\mathcal{K} = 3c^2 M_p^2$ for the standard holographic dark energy case. We can do the same procedure for the other two remaining models, but using the horizon for the Tsallis model, given by

$$\int_x^{\infty} \frac{dx}{Ha} = \frac{1}{a}\left(\frac{\mathcal{K}}{3M_p^2 H^2 \Omega_{de}}\right)^{\frac{1}{2(2-\delta)}}, \tag{3.42}$$

where $x = ln(a)$. The differential equation associated is

$$\boxed{\frac{\Omega'_{de}}{\Omega_{de}\left(1-\Omega\right)} = 2\delta - 1 + Q_{\mathcal{T}}\left(1-\Omega_{de}\right)^{\frac{1-\delta}{2(2-\delta)}}\left(\Omega_{de}\right)^{\frac{1}{2(2-\delta)}} e^{\frac{3(1-\delta)}{2(2-\delta)}x},} \tag{3.43}$$

where

$$Q_{\mathcal{T}} = 2(2-\delta)\left(\frac{N}{3M_p^2}\right)^{\frac{1}{2(\delta-2)}}\left(H_0\sqrt{\Omega_{m0}}\right)^{\frac{1-\delta}{\delta-2}}.$$

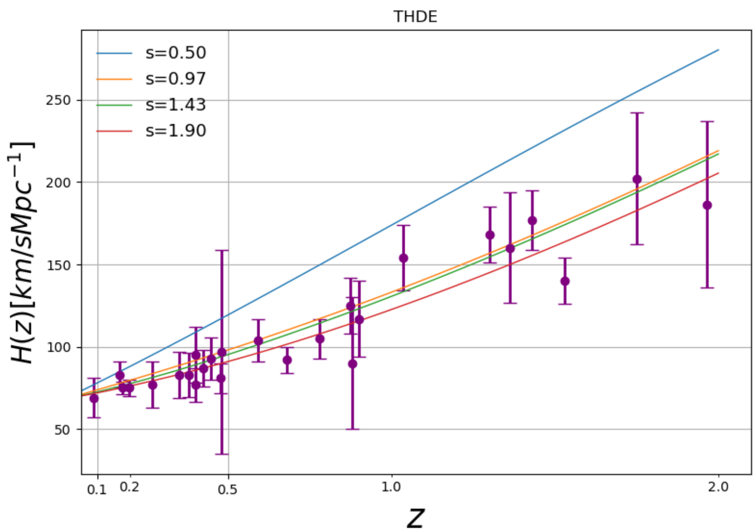

Figure 3.4: The Hubble factor $H(z)$ with redshift z, in units when $M_p^2 = 1$ and $H_0 = 70$. To be consistent with data, we use the initial condition $\Omega_{de}(z=0) = 0.7\,\mathrm{km/s/Mpc}$.. The bars represent the 26 $H(z)$ data points.

In this model, the EoS parameter is given by [55]

$$\omega_{\rm de} = \frac{1-2\delta}{3} - \frac{Q}{3}\left(\Omega_{\rm de}\right)^{\frac{1}{2(2-\delta)}}\left(1-\Omega_{\rm de}\right)^{\frac{\delta-1}{2(\delta-2)}} e^{\frac{3(1-\delta)}{2(\delta-2)}x}. \tag{3.44}$$

As you can note, the Barrow and Tsallis cases are very similar if we consider $\delta \longrightarrow 1 + \mathcal{B}/2$. For the above reason, in Barrow's case, Tsalli's differential equation can be reduced to standard holographic dark energy.

For the case of the Tsallis Holographic Dark Energy Model, since we have two free parameters at the beginning, we must set one ($c = 1.0$) and vary the other (δ). As you can see in the figure 3.4, the value $\delta = 0.5$ is completely outside the data region of $H(z)$, so we can consider $\delta \leq 0.5$ disposable values. On the other hand, we can see that the values closest to ΛCDM are $\delta \approx 2.0$, so we can consider exploring the region $0.5 \leq \delta \leq 2.5$.

3.6 Generalized holographic model

As we saw earlier, the Tsallis and Barrow models share many similarities, so we can switch from one model to another by choosing the parameters correctly. Similarly, we have seen how these models recover HDE and LCDM in the appropriate limits. However, to find even more general models that could better fit the observational data, we can consider that the exponent present in the entropy may be a function of some of our cosmological parameters. This idea is inspired by the recent work of Basilakos et al. [57] In this case, we consider generalizing the Tsallis model. For this, consider the following entropy

$$S_G = \Lambda A^{f(x)}, \tag{3.45}$$

where Λ is constant, and $f(x)$ is a function that for some value x_0 we will get $f(x_0) = 1$, so in this case $S_G \sim S_{BK}$. Also, the dark energy density in this case is

$$\rho_{de} = \lambda L^{2(f(x)-2)}, \tag{3.46}$$

as we can see in the case for $\lambda = 3M_p^2c^2$ and $f(x_0) = 1$, the expression (3.46) becomes in the standard holographic dark energy case. In the same way, if $f(x_2) = 2$ for some x_2, is the case of model ΛCDM i.e. a dark energy density constant, and for all cases $f(x_c)$ constant, we will get the Barrow and Tsallis models.
In this case, the horizon's integral is

$$\int_x^\infty \frac{dx}{Ha} = \frac{1}{a}\left(\frac{\lambda}{3M_p^2H^2\Omega_{de}}\right)^{\frac{1}{2(2-f(x))}}, \tag{3.47}$$

now if we derivate the expression (3.47), we can find an equation for the evolution of the generalized holographic dark energy. This equation is

$$\begin{aligned}\frac{\Omega'_{de}}{\Omega_{de}(1-\Omega_{de})} = \frac{2\sqrt{\Omega_{de}}}{c}\left(\frac{Q_G(x)(1-\Omega_{de})}{\Omega_{de}}\right)^{\frac{f(x)-1}{2(f(x)-2)}}(2-f(x)) + 2f(x)\\ - 1 + \log\left(\frac{Q_G(x)(1-\Omega_{de})}{\Omega_{de}}\right)^{\frac{f'(x)}{f(x)-2}},\end{aligned} \tag{3.48}$$

where

$$Q_G(x) = \frac{c^2 e^{3x}}{H_0^2 \Omega_{m,0}}. \tag{3.49}$$

In the same way, the equation-of-state parameter associated with this general case is

$$\begin{aligned}\omega_{de} = -\frac{2f(x)-1}{3} + \frac{2(f(x)-2)\sqrt{\Omega_{de}}}{3c}\left(\frac{Q_G(x)(1-\Omega_{de})}{\Omega_{de}}\right)^{\frac{f(x)-1}{f(x)-2}} \\ -\frac{2f'(x)}{3}\left(\log\frac{Q_G(x)(1-\Omega_{de})}{\Omega_{de}}\right)^{\frac{1}{2(2-f(x))}},\end{aligned} \tag{3.50}$$

from this expression, you can notice that in the case when $f(x) \longrightarrow 1$, is the case of the standard holographic dark energy, and in the case when $f(x) = 2$, is the Λ CDM case, i.e. $\omega_{de} = -1$. Likewise, notice that is convenient to rewrite this equation as a function of z, for this, consider $f(x) \longrightarrow f(z)$ and $f'(x) = -(1+z)\frac{df}{dz}$, thus the equation (3.48) takes the form

$$\begin{aligned}-\frac{(1+z)}{\Omega_{de}(1-\Omega_{de})}\frac{d\Omega_{de}}{dz} = \frac{2\sqrt{\Omega_{de}}}{c}\left(\frac{Q_G(z)(1-\Omega_{de})}{\Omega_{de}}\right)^{\frac{f(z)-1}{2(f(z)-2)}}(2-f(z)) + 2f(z) \\ -2+\log\left(\frac{Q_G(z)(1-\Omega_{de})}{\Omega_{de}}\right)^{\frac{-(1+z)f'(z)}{f(z)-2}},\end{aligned} \tag{3.51}$$

where in this case

$$Q_G(z) = \frac{c^2}{H_0^2 \Omega_{m,0}(1+z)^3}. \tag{3.52}$$

3.6.1 Linear dependence on the exponent

Notice that $f(z)$ is an unspecific function so far, thus, we have "more freedom" to choose the exponent expression (any chosen function should satisfy the entropy properties mentioned above), and due to one of the most important properties of the entropy is the monotonically increasing behavior, we can guarantee that considering the exponent as a linear function in a general way such as $f_l(z) = a + bz$ (with a and b constants), we can see that for the case $f(0) = a$, is the Barrow and Tsallis cases, i.e. when the exponent is constant. Using the linear function in the expression, (3.51) the evolution of the dark energy parameter density is given by

$$-\frac{(1+z)}{\Omega_{de}(1-\Omega_{de})}\frac{d\Omega_{de}}{dz} = \frac{2\sqrt{\Omega_{de}}}{c}\left(\frac{Q_G(z)(1-\Omega_{de})}{\Omega_{de}}\right)^{\frac{a+bz-1}{2(a+bz-2)}}(2-a-bz) + 2(a+bz) - 2 + \log\left(\frac{Q_G(z)(1-\Omega_{de})}{\Omega_{de}}\right)^{\frac{-(1+z)b}{a+bz-2}}, \tag{3.53}$$

From this equation, we can see that the values $a = 1$ and $b = 0$ take the form of the standard holographic dark energy case. From the figure 3.5, we can see the effect of the dependence on z in our exponent, for this plot, we fixed $a = 0.4$ and $c = 1$. Notice that the effect of the linear dependence is indivisible at $z = 0.5$, but at $z = 2$ the solutions are considerably different from each other, so at high redshift, the contribution by the linear parameter is relevant, for example, if we want to use data sets from Microwave Cosmic Background, these contributions are significant.

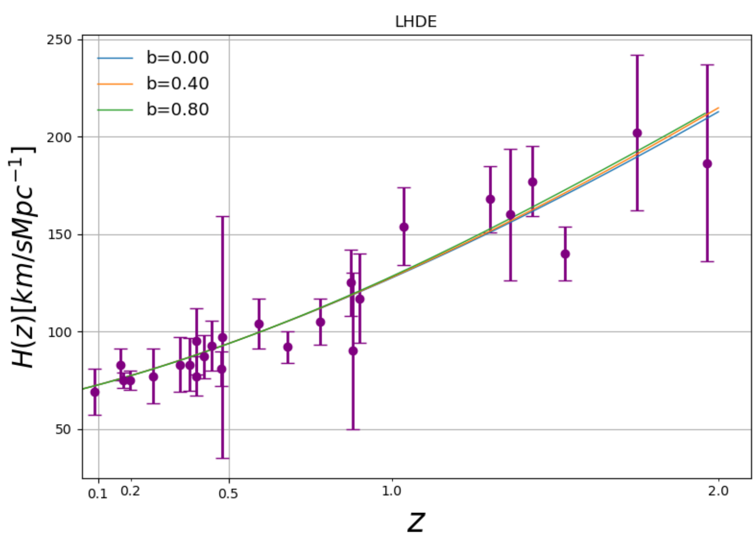

Figure 3.5: Hubble parameter for the linear case

3.6.2 Trigonometric dependence on the exponent

As we mentioned before, there are many reasons to generalize our standard holographic model of dark energy. In this case, the proposed exponent in our general expression of entropy is motivated from an observational aspect, since recently through reconstruction processes of the equation of state of dark energy only through observational data (free from models), it seems to present an oscillation (see figure 3.6). Likewise, from the equation of state (3.50), we have a fundamental model where, if the general function $f(x)$ or $f(z)$ is the appropriate, ω_{de} can oscillate. For these reasons, consider the function $f(z) = k + rsin(z)$, thus, the evolution of the dark energy in this case is given by

$$\begin{aligned}-\frac{(1+z)}{\Omega_{de}(1-\Omega_{de})}\frac{d\Omega_{de}}{dz} = \frac{2\sqrt{\Omega_{de}}}{c}\left(\frac{Q_G(z)(1-\Omega_{de})}{\Omega_{de}}\right)^{\frac{k+rsin(z)-1}{2(k+rsin(z)-2)}}(2-k-rsin(z))\\ +2(k+rsin(z))-2+\log\left(\frac{Q_G(z)(1-\Omega_{de})}{\Omega_{de}}\right)^{\frac{-(1+z)rcos(z)}{k+rsin(z)-2}}\end{aligned} \tag{3.54}$$

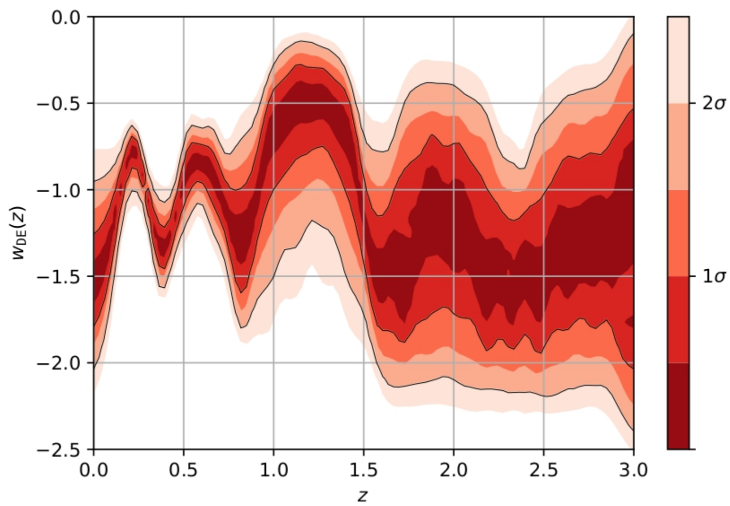

Figure 3.6: The reconstructed equation of state for dark energy by Escamilla, L. A. et al. *Oscillations in the Dark?*[58]

.

Chapter 4

Bayesian statistics

Bayesian statistics is an approach that relies on the Bayesian interpretation of probability, where probability is conceived as a measure of uncertainty or degree of belief regarding the occurrence of an event. Unlike frequentist statistics, which focuses on the relative frequency of long-term events, Bayesian statistics integrates prior information (called a priori information) with observed evidence to update beliefs and make inferences about model parameters or predictions.

4.1 Theorem of Bayes

For two events A and B, the theorem of Bayes establishes the relation

$$P(B|A) = \frac{P(A|B)P(B)}{P(A)}, \tag{4.1}$$

where $P(A|B)$ is the probability of event A occurring given that event B has occurred, known as *the posterior probability*. $P(B|A)$ is the probability of the event B ocurring given that event A has occurred, it is know as *likelihood*. $P(A)$ is the a priori probability of event A i.e., the probability that A occurs before B is observed and the analogous form for $P(B)$.
In the Bayesian framework, the data and the model are in the same space. For this reason, for a given model H (hypothesis), we consider D as A, i.e., a set of data. In the same way, we consider

θ as B i.e. the parameter vector of said hypothesis. The theorem of Bayes takes the form

$$\boxed{P(\theta|D,H) = \frac{P(D|\theta,H)P(\theta|H)}{P(D|H)},} \tag{4.2}$$

where

- Is usually express the likelihood as $L(D|\theta,H) = P(D|\theta,H)$.
- The prior as $\pi(\theta) = P(\theta|H)$, is the knowledge about the model.
- And $\mathcal{Z} = P(D|H)$ is the evidence of the model, usually know as *Bayesian Evidence.*

The Bayesian Evidence can be calculated from the formula

$$\mathcal{Z} = \int d^N\theta P(D|\theta,H)P(\theta|H). \tag{4.3}$$

In this espression we consider a parameter space with dimension N. The Bayesian evidence is crucial in determining the model that most accurately represents the data, a process commonly referred to as model selection. For this reason, is useful to define the ratio of the two evidence

$$K \equiv \frac{P(D|H_1)}{P(D|H_2)} = \frac{\mathcal{Z}_1}{\mathcal{Z}_2}. \tag{4.4}$$

From this definition, we can define another quantity known as *Bayes factor*

$$\mathcal{B}_{1,2} = \ln(K) = \ln(\mathcal{Z}_1/\mathcal{Z}_2), \tag{4.5}$$

This factor provides an insight into the extent to which Model 1 might adequately explain the data in comparison to Model 2, for example. The significance of Bayes' theorem in statistical inference is immense. In conventional practice, we often gather data and interpret it using a predefined model. However, the inverse is often true: we initially possess a dataset and then assess various models' suitability based on the probability of fitting the data. Bayes' theorem offers a mechanism to bridge these two approaches. By leveraging Bayes' theorem, we can effectively determine the model that most accurately aligns with the observed data. For a better interpretation of the Bayes factor, the *Jeffreys guideline scale* is used to measure the comparative evidence supporting one model over another (see Table 4.1). This criterion can be summarized as follows

Jeffreys guideline scale			
$\lvert\mathcal{B}_{1,2}\rvert$	**Odds**	**Probability**	**Strength**
> 5.0	$> 150:1$	> 0.993	Decisive
$2.5 - 5.0$	$\sim 150:1$	0.993	Strong
$1.0 - 2.5$	$\sim 12:1$	0.923	Significant
< 1.0	$< 3:1$	0.750	Inconclusive

Table 4.1: Jeffreys guideline scale.

For our purposes, this criterion is of utmost importance, as we can directly compare a reference model in cosmology like ΛCDM with one of our holographic models and see how well it fits the data.

4.2 Likelihood

As mentioned earlier, when we are only interested in analyzing a single model, Bayesian evidence is not very relevant, as it can be absorbed in the normalization of the posterior. This is why the likelihood plays an important role in comparing our models with observational data.
In this way, if we maximize the likelihood, we can find the most probable parameter's set, because $P(\theta|D,H) \propto \mathcal{L}(D|\theta,H)$ and with $P(D|H) = 1$. Based on the above, we are interested in understanding the effects of maximum likelihood when compared to the likelihood at a particular point in parameter space, we define the likelihood ratio as follows

$$\mathcal{R} = -2\ln\left(\frac{\mathcal{L}(D|\theta,H)}{\mathcal{L}_{max}}\right), \tag{4.6}$$

From this definition, we can consider that some parameters are acceptable if this ratio exceeds the given value.

Now, consider a Taylor expansion around the maximum

$$\ln \mathcal{L}(D|\theta) = \ln \mathcal{L}(D|\theta_0) - \frac{1}{2}(\theta_i - \theta_{0i})H_{ij}(\theta_j - \theta_{0j}) + \dots \tag{4.7}$$

or

$$\mathcal{L}(D|\theta) = \mathcal{L}(D|\theta_0)\exp\left(-1/2(\theta_i - \theta_{0i})H_{ij}(\theta_j - \theta_{0j})\right) \tag{4.8}$$

where for the mean of the distribution $\hat{\theta}$, due to our models are well-specified, the expectation value is the real value, i.e. $\langle\hat{\theta}\rangle = \theta_0$, and H_{ij} is known as *Hessian matrix*, defined as

$$H_{ij} = -\frac{\partial^2 \ln \mathcal{L}}{\partial\theta_i \partial\theta_j}.$$

From this matrix, we can know if the parameters θ_i and θ_j are correlated, because if this matrix is diagonal ($H_{ij} = 0$ for $i \neq j$), the parameters are uncorrelated. Notice, in this case, we use the Hessian language due to around the maximum posterior, the posterior distribution can be approximated through a Gaussian distribution, thus, the inverse of the Hessian at this point performs as an estimation of the covariance matrix of parameters. This means, that even the Hessian and the covariance matrix are related, the first is more useful during the optimization and approximation processes.

4.3 Chi-square

If we decide to use the Gaussian approximation (4.8), we will get the maximum likelihood when the quantity [1]

$$\chi^2 = (\theta_i - \theta_{0i})H_{ij}(\theta_j - \theta_{0j}), \tag{4.9}$$

is minimum, this quantity is known as *chi-square* and is one of the most important criteria to test a model with data sets. Is important to notice that not always the likelihood can be described by Gaussian distribution, so in this case, the likelihood and the χ^2 are not equivalent.

[1] When we have many observations or data, the central limit theorem ensures that, under certain conditions, the distribution of the estimators (i.e., the posterior distribution of the parameters) will approach a normal (Gaussian) distribution, regardless the form of the original distribution.

4.3.1 Confidence regions

After obtaining the best-fit parameters (minimum chi-square), we aim to identify confidence regions where values can be deemed suitable candidates for our model. The most reasonable approach is to select values within a compact region around the best-fit value.
Consider the interval from the best fit (bf) to another value of the chi-square, i.e.

$$\Delta\chi^2 = \chi^2 - \chi^2_{bf},$$

so usually the confidence regions from this variation to the minimum Chi-square are categorized by the sigma-notation. For Gaussian distributions, the 1σ, 2σ, and 3σ cases the confidence levels as a function of the number of parameters M are 68.3%, 95.4% and 99.73% respectively.

4.4 Markov Chain Monte Carlo

Monte Carlo simulation is a computational technique used to estimate outcomes by generating multiple random samples from a probability distribution and then analyzing those samples to obtain information about the system under study. The fundamental idea behind Monte Carlo simulation is to use the principle that, if enough random samples are generated from a given probability distribution, the distribution of the results of those samples will converge to the underlying probability distribution. This allows for estimating quantities of interest, such as the expected value, variance, percentiles, among others. In addition, a Markov Chain is a stochastic process that moves between different states in discrete time steps. Transition probabilities determine these state changes, relying solely on the current state and not on the past sequence of states. In essence, it's a memoryless random process governed by the Markov property, indicating that the system's future behavior is solely dependent on its current state, regardless of its history.
Combining these two important ideas, the basic idea behind Markov Chain Monte Carlo (MCMC) is to generate a sequence of samples from a given probability distribution, such that the distribution of the samples converges to the desired distribution. This is achieved by constructing a Markov chain whose stationary probabilities match the target distribution. Through an iterative process, the Markov chain moves through the parameter space, generating samples that eventually

converge to the distribution of interest.
For these reasons, if we consider a *target density*, it can be approximated by delta functions [59]

$$p(\theta|D,H) \simeq \frac{1}{N}\sum_{i=1}^{N}\delta(\theta-\theta_i), \tag{4.10}$$

from this approximation, we can estimate some integral in the way

$$\langle f(\theta)\rangle \simeq \frac{1}{N}\sum_{i=1}^{N} f(\theta_i) \tag{4.11}$$

Since in this process to generate a new point in our parameter space, it is necessary to know the previous one (and only this one), we must have a rule that allows us to know if the next step is better than the previous one, (otherwise we will never optimize our process), for this reason, the acceptance criteria are very necessary. In MCMC the algorithm that provides this criterion, which is the simplest, and therefore, the most used, is known as the Metropolis-Hastings algorithm [60].

The steps of this algorithm are usually the following:

1. Compute the posterior distribution for a random point in the parameter space θ_0.

2. From a proposal distribution in the parameter space, generate a new point θ_n and calculate its posterior distribution.

3. Reject or accept the new point using

   $$p(acceptance) = min\left[1, \frac{p_n}{p_0}\right],$$

   where p_i and p_n are the posterior probabilities of the initial point θ_0 and θ_n, respectively.

4. If the point is rejected, revert to the previous point in the chain and repeat the process.

5. Repeat the process of steps 2 to 4 to have a large enough chain.

The MCMC algorithm and its variants have been extensively studied and applied across a wide range of problems. Its effectiveness and versatility make it an invaluable tool for statistical inference and data analysis in situations where direct computation of probability distributions is difficult or impossible.

4.5 Nested Sampling

The Nested Sampling algorithm is a type of Monte Carlo to calculate an integral over a given parameter space given a model. The desired function to be integrated is the Likelihood function $\mathcal{L}(D|\theta, H)$ which is "marginalized" on our parameter space, according to our prior $\pi(\theta)d\theta$. This integral over the total parameter space is given as,

$$Z = \int \mathcal{L}(D|\theta, H)\pi(\theta)d\theta, \tag{4.12}$$

which is known as the marginalized likelihood or Bayesian evidence. Similarly, recall that the Bayes factor is the radius of the Bayesian likelihoods of two different models.
The Nested Sampling algorithm is mainly composed of the following sections, [61]:

1. **Initialization:** In this first step of the algorithm, we perform a random sampling from our prior N live points and evaluate the likelihood for each point.

2. **Shrinkage:** During this stage, the live point with the worst likelihood $\mathcal{L}_1$ is removed, i.e. the worst fit. This removed point becomes the first dead point. Note that each point sampled represents a fraction of the total volume $(1/N)$, thus by eliminating the dead point, our volume is reduced by a factor of $\delta V \sim 1/N$ approximately. This volume variation estimator can change according to the needs and is an area of interest in itself.

3. **Likelihood-restricted prior sampling (LRPS):** Since the dead point was removed, it is necessary to add a new live point, to do this, it is necessary to sample a new point from our prior and also impose the condition that our new live point has a higher associated likelihood compared to $\mathcal{L}_1$.

4. **Iterations:** Once the first steps have been established, it is necessary to repeat the same process numerous times, so after a certain number i of iterations the volume removed is

exponentially small, i.e, $V_i = \left(1 - \frac{1}{N}\right)^i$, during this process the likelihood of the removed points tends to be flat.

5. **Integration:** Since removing a point in turn reduces the volume as mentioned above, the volume difference can be estimated using

$$\Delta V_i = V_i - V_{i-1} = \left(1 - \frac{1}{N}\right)^i \times \frac{1}{N}, \tag{4.13}$$

Because for each dead point, we will have a non-normalized weight $\Delta V_i \times L_i$ associated with it. It is thus possible to estimate the Bayesian evidence integral in the form

$$Z \approx \sum_i \Delta V_i \times \mathcal{L}_i, \tag{4.14}$$

Note that weighted dead points can be sampled approximately from the posterior and for convenience resampled proportionally to $\Delta V_i \times \mathcal{L}_i$, in subsequent unweighed samples.

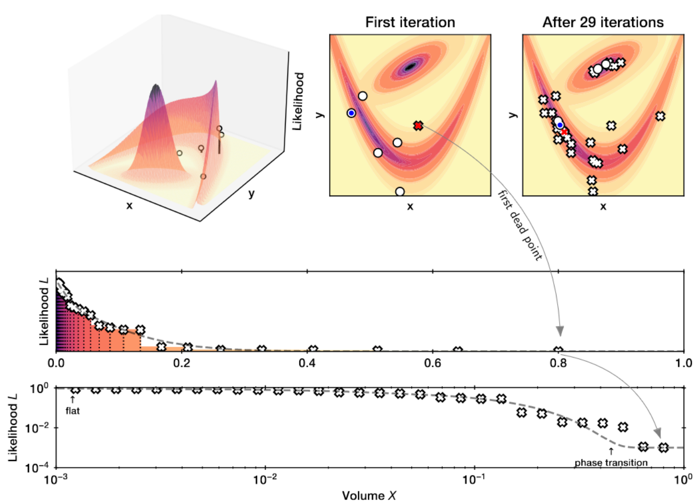

Figure 4.1: Graphic representation of the steps described, as you can see that the likelihood of the dead points tends to be flatter as the volume is reduced [62].

As we can see from the Figure 4.1, the likelihood function is defined over a two-dimensional parameter space. Following the steps mentioned above, the Nested Sampling algorithm starts by evaluating the random points in the parameter space, in this case, $N = 5$, each live point is shown in turn defines a likelihood contour which is marked with circles, thus the point with the lowest likelihood (red cross) becomes the first dead point. This point is replaced by a new live point (blue point) which is sampled using the prior. Following the process, a certain number of iterations are performed, in which a dead point is replaced with a new live point whose likelihood is higher and higher. This ensures that the likelihood of the new point is increasing until it reaches a maximum value, where regardless of the number of iterations the value does not change. This likelihood maximization in turn is reflected in the reduction of the volume of our parameter space as we can see, making the points tend to cluster in regions where the likelihood is higher, so this algorithm is called Nested Sampling.

Chapter 5

Results

5.1 Observational data sets

5.1.1 Cosmic chronometers

The first data set used in this analysis is the *cosmic chronometers*, which relies on the differential age of galaxies. In this frame, the expansion rate is given by

$$H(z) = \frac{\dot{a}}{a} = -\frac{1}{1+z}\frac{dz}{dt}, \tag{5.1}$$

notice that the term dz is derived from highly accurate spectroscopic surveys, requiring only the measurement of the differential age evolution of the Universe, i.e. dt for some redshift interval. As we can see, a direct cosmology-independent measurement of the Hubble parameter, is given by a measure of dt.

In this project, we used a total set of 31 measurements of the Hubble parameter by the cosmic chronometers approach; 8 measures in the redshift range $0.15 < z < 1.1$ from the differential spectroscopic evolution of early-type galaxies as a function of redshift with a precision of the $5 - 12\%$ mapping homogeneously the redshift range up to $z \sim 1$ [63], 8 values of the $H(z)$ in the redshift range $0.1 < z < 1.8$ using observations of passively evolving galaxies and supernova data [64], 2 measures at $z \approx 0.5$ and $z \approx 0.8$ [65] and 5 measures in the range $0.3 < z < 0.5$ [66]. These points are shown in figure 5.1 and the Hubble parameter described by the ΛCDM model.

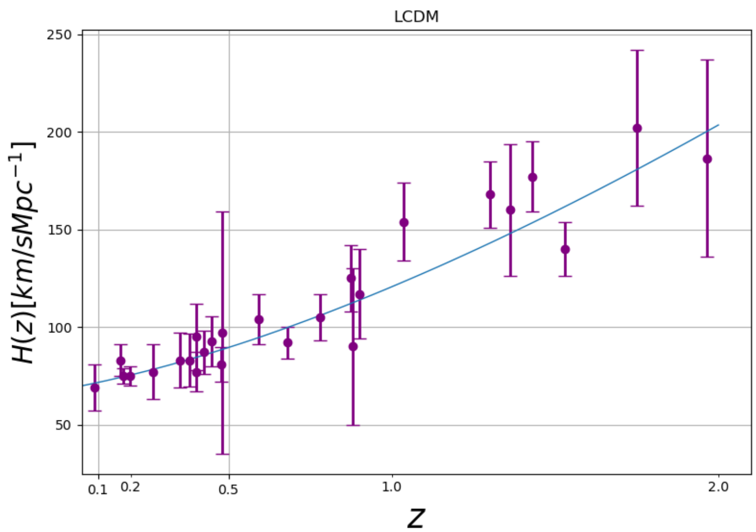

Figure 5.1: 31 data points of the Hubble parameter with its errors and Hubble parameter by ΛCDM model.

5.1.2 Supernovas

Another sample used in this analysis consists of SN Ia light curves, which include data from the complete three-year span of the SDSS survey, and the remainder of our sample is the "C11 compilation". This compilation contains SNe from SNLS, HST, and several nearby experiments. This extended sample of 740 SNe Ia is known as the *JLA* sample, and we just used 31 binned points from JLA[67].

The SDSS-II (Sloan Digital Sky Survey II) Supernova Survey was a key project aimed at discovering and studying Type Ia supernovae (SNe Ia) to better understand the nature of dark energy and the expansion of the universe. The SDSS-II survey, which operated from 2005 to 2008, focused on intermediate redshift supernovae ($0.05 < z < 0.4$), bridging the gap between nearby and high-redshift supernovae. This survey served as an effective low-redshift anchor for the Hubble diagram, which plots the distance versus redshift of supernovae. Furthermore, this anchoring is crucial for reducing systematic errors from calibration systematics in the low-redshift SN sample and improving the overall accuracy of cosmological measurements. The JLA sample includes a selection of 374 SNe Ia from this spectroscopic sample. On another hand, the *C11 compilation*, includes supernovae data from multiple sources: the Supernova Legacy Survey (SNLS), the Hubble Space Telescope (HST), and several nearby experiments. The C11 compilation is considered integral to the analysis because it provides a robust and extensive dataset that enhances the statistical power and accuracy of cosmological parameter estimation. This compilation is about 242 spectroscopically confirmed SNe Ia from the first three seasons of the five-year SNLS survey ($0.2 < z < 1.0$).

5.1.3 Barionic acustic oscilations

The last data set used is baryon acoustic oscillations (BAO). The BAO scale is defined by the radius of the sound horizon from the drag epoch z_d, which is when the photons and baryons decouple. This radius is given by

$$D_d = \int_{z_d}^{\infty} \frac{c_s(z)}{H(z)} dz,$$

where

$$c_z(z) = \frac{c}{\sqrt{3\left(1 + \frac{3}{4}\rho_b(z)/\rho_\gamma(z)\right)}}.$$

Notice that in a measurement of $\alpha_\perp$ (the ratio perpendicular to the line of sight) from clustering at z constraints, the ratio of the comoving angular diameter distance to the sound horizon is given by

$$\frac{D_M(z)}{r_d} = \alpha_\perp \frac{D_{M,\text{fid}}(z)}{r_{d,\text{fid}}}, \tag{5.2}$$

where $D_{M,\text{fid}}(z)$ is the fiducial comoving angular diameter distance, i.e. the comoving angular diameter distance in a specific cosmological model (fiducial cosmology). In the same way, a measurement of $\alpha_\parallel$ (the ratio parallel to the line of sight) constrains the Hubble parameter $H(z)$, which we convert to an analogous quantity

$$D_H(z) = \frac{c}{H(z)}, \tag{5.3}$$

with

$$\frac{D_H(z)}{r_d} = \alpha_\parallel \frac{D_{H,\text{fid}(z)}}{r_{d,\text{fid}}}. \tag{5.4}$$

Now notice that an isotropic BAO analysis measures an effective combination of these two distances. When redshift-space distortions are weak (a reasonable approximation for luminous galaxy surveys after reconstruction though not for the LyaF), the constrained quantity is the volume-averaged distance, i.e.

$$D_V = \left(zD_H(z)D_M^2(z)\right)^{1/3},$$

where

$$\frac{D_V(z)}{r_d} = \alpha \frac{D_{V,\text{fid}}(z)}{r_{d,\text{fid}}} \tag{5.5}$$

The data set for BAO used in this work comes from galaxy clustering measurements and the Lyman-α forest (LyaF) obtained by the Baryon Oscillation Spectroscopic Survey (BOSS) of SDSS-III (Sloan Digital Sky Survey). These measurements are made using measuring the BAO distance scale with one-percent precision from a redshift survey of 1.5 million luminous galaxies at $z = 0.2$ to 0.7 and making the first BAO measurement at $z > 2$ by 3-dimensional structure in the Lyα forest absorption towards a dense grid of 160,000 high-redshift quasars [68]. These constrain values are shown in table 5.1

Data	D_V/r_d	D_M/r_d	D_H/r_d	z
6dFGS	3.047 ± 0.137	-	-	0.106
MGS	4.480 ± 0.168			0.15
BOSS LOWZ Sample	8.467 ± 0.167	–	–	0.32
BOSS CMASS Sample	–	14.945 ± 0.210	20.75 ± 0.73	0.57
LyaF auto-correlation	–	37.675 ± 2.171	9.18 ± 0.28	2.34
LyaF-QSO cross correlation	–	36.288 ± 1.344	9.00 ± 0.30	2.36
Combined LyaF	–	36.489 ± 1.152	9.145 ± 0.204	2.34

Table 5.1: **BAO constraints:** These values are from [68].

5.2 Results

From the priors studied in Chapter 3, for each parameter in the different models, we realize parameter inference using data sets from Baryonic acoustic oscillations, cosmic chronometers, and Supernovas, described above. For the parameter's inference, we used the Nested Sampling algorithm above described in the Python library `SimpleMC`. The values of the new parameters in the holographic dark energy models are shown in the table 5.2 the triangle plots for each model with the posterior distributions are in Appendix A.

Models	Parameters	Value
HDE	c	0.8877 ± 0.1004
$\mathcal{B}$HDE	c	1.5387 ± 0.2580
	$\mathcal{B}$	0.2566 ± 0.0786
$\mathcal{T}$HDE	c	1.2405 ± 0.4551
	δ	1.1287 ± 0.0555
$\mathcal{L}$HDE	c	1.2295 ± 0.4537
	a	-0.1272 ± 0.2653
	b	-0.0657 ± 0.2481
$\mathcal{S}$HDE	c	0.8955 ± 0.1693
	k	0.1079 ± 0.0561
	r	0.1125 ± 0.0539

Table 5.2: **Holographic parameters**

As you can see, the holographic parameter values are proximally the theoretically expected values, except for the linear holographic model, where, as we can notice, the values of the exponents are negative, this is an important result because theoretically, the exponents should be positive to have an increasing entropy function, however, the observational data used prefer negative values. Notice that for each holographic case, we performed tests with extended priors that could include negative values to confirm the exponent's positivity, however, for all cases the exponent's best-fit values were found positive except the linear-exponent case.

In figure 5.2 are shown the confidence regions for the holographic models and ΛCDM, as you can see, the areas for the cosmological values agreed with the cosmological standard model, however, it is noteworthy that the $\mathcal{L}$HDE model seems to contain the ΛCDM confidence regions more completely than the other models, as we can see in Figures (a), (b) and (c). I used the Python package `GetDist` for analyzing and plotting Monte Carlo (or other) samples [69]. On the other hand, the standard holographic model seems slightly more distant from the ΛCDM regions in the 3 figures above, which is to be expected, since it is a non-generalized holographic dark energy model with a fixed exponent value.

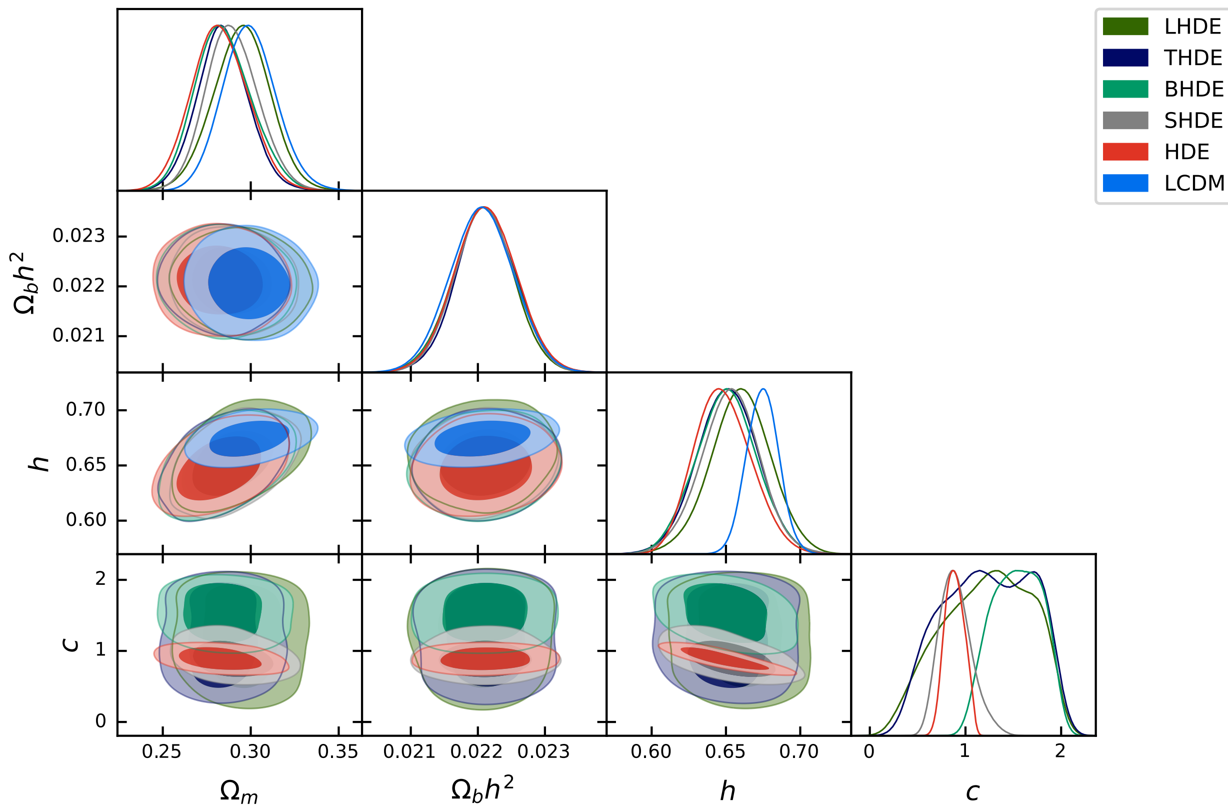

Figure 5.2: Confidence regions and probability distributions of the holographic models and ΛCDM model.

The case of the c parameter, from the table is the 5.2, all values are around 1, in figure 2.2 (d), we can see that just two confidence regions are well constrained, the $\mathcal{S}$HDE and HDE cases, while, there are constriction problems with the other models, possibly due to the correlation between the parameters or the types of data used. It is important to note that the $\mathcal{S}$HDE and HDE regions are very poorly related to BHDE since these models prefer values less than 1 and the other one greater than 1. For all the holographic models, the same prior was used for parameter c, which was $0.5 \leq c \leq 2.0$.

Table 5.3 shows the cosmological parameters and statistical criteria for ΛCDM and holographic dark energy models. We can notice that compared to ΛCDM the values of h ($H_0/100$) are smaller than expected, this could be because the observational data used are local. This result indicates that the holographic dark energy models do not relieve the strain of H_0 compared to ΛCDM.

Models	$\Omega_{m,0}$	$\Omega_{b,0}h^2$	h	ΔAIC	χ^2	$\|\mathcal{B}\|$
ΛCDM	0.2991 ± 0.0152	0.0221 ± 0.0005	0.6746 ± 0.0107	-	61.31	-
HDE	0.2979 ± 0.0161	0.0221 ± 0.0005	0.6551 ± 0.0196	3.33	62.55	1.54
$\mathcal{B}$HDE	0.2833 ± 0.0160	0.0221 ± 0.0004	0.6488 ± 0.0217	4.63	61.88	1.81
$\mathcal{T}$HDE	0.2841 ± 0.0145	0.0221 ± 0.0004	0.6511 ± 0.0200	4.31	61.87	2.69
$\mathcal{L}$HDE	0.2948 ± 0.0160	0.0221 ± 0.0004	0.6599 ± 0.0203	2.87	58.12	2.2
$\mathcal{S}$HDE	0.2895 ± 0.0148	0.0221 ± 0.0004	0.6527 ± 0.0197	2.73	59.16	1.24

Table 5.3: Cosmological parameter values and statistical criterions.

On the other hand, concerning the statistical criteria, there are holographic dark energy models that fit better with the observational data used. As we note, the case of the generalized exponent models presents a lower χ^2 than ΛCDM, in particular, the linear LHDE model has the lowest chi compared to the other models. Note that the importance of which linear model is the best fit to the data is greater when we remember that the values of the inferred parameters of the generalized exponent $f(z) = -0.1272 \pm 0.2653 + (-0.0657 \pm 0.2481)z$ are negative, which is something that is theoretically ruled out in the Barrow model. Similarly, compared to the ΛCDM model, using Jeffrey's guideline from table 4.1, we can note that the strength is significant, i.e., the observational data used significantly or slightly favors ΛCDM, as in all holographic models except for the Tsallis model.

In figures 5.3 and 5.4, we present the regions of 1σ and 2σ for the $\Omega_{de}(z)$, $\omega_{de}(z)$ and $q(z)$ parameters were calculated using the `fgivenx` package [70] for plotting posteriors of functions, using our chains for each holographic model.

First, we can note that the dark energy density parameter has a similar behavior for all holographic models. However, in the special case of the linear model represented in Figure 2.4 (d), this parameter density decays faster than the rest of the models. On the other hand, in the $\omega_{de}(z)$ case, we can note a clear difference in the plots for some models, as is the case of the generalized exponent cases, this is due to the general expression for these models is proportional to the function of the generalized exponent, thus, if we choose an oscillating function, that oscillation will be present in the $\omega(z)$, we introduced this idea in the chapter 3 to explain the oscillations presents in the reconstruction of the dark energy density, in this case, we just get one oscillation for some period

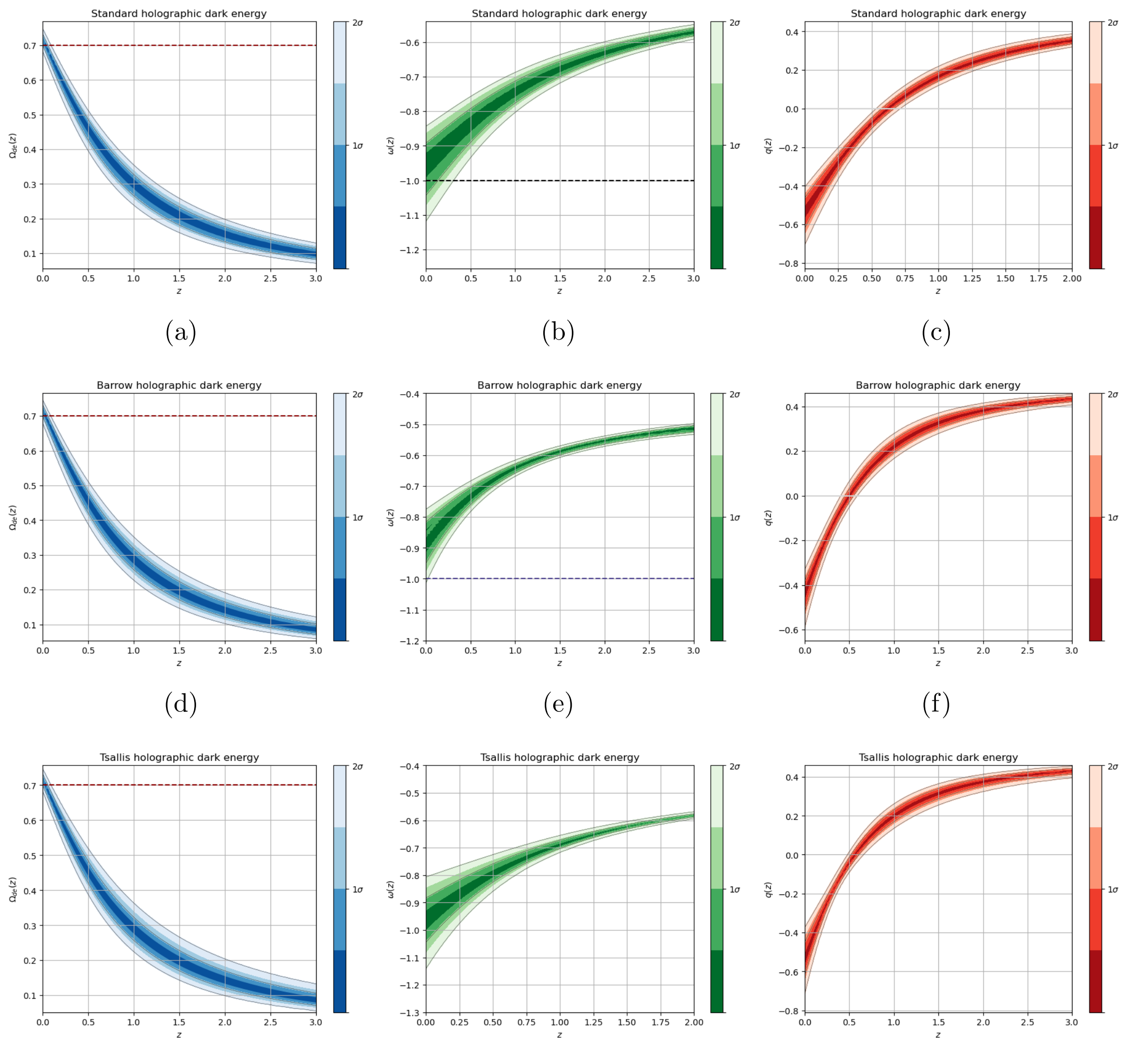

(a) (b) (c)

(d) (e) (f)

(g) (h) (i)

Figure 5.3: 1σ and 2σ regions for the Ω_{de}, $\omega_{de}(z)$, and $q(z)$ for standard holographic dark energy (HDE), Barrow holographic dark energy ($\mathcal{B}$HDE) and Tsalis holographic dark energy $\mathcal{T}$HDE.

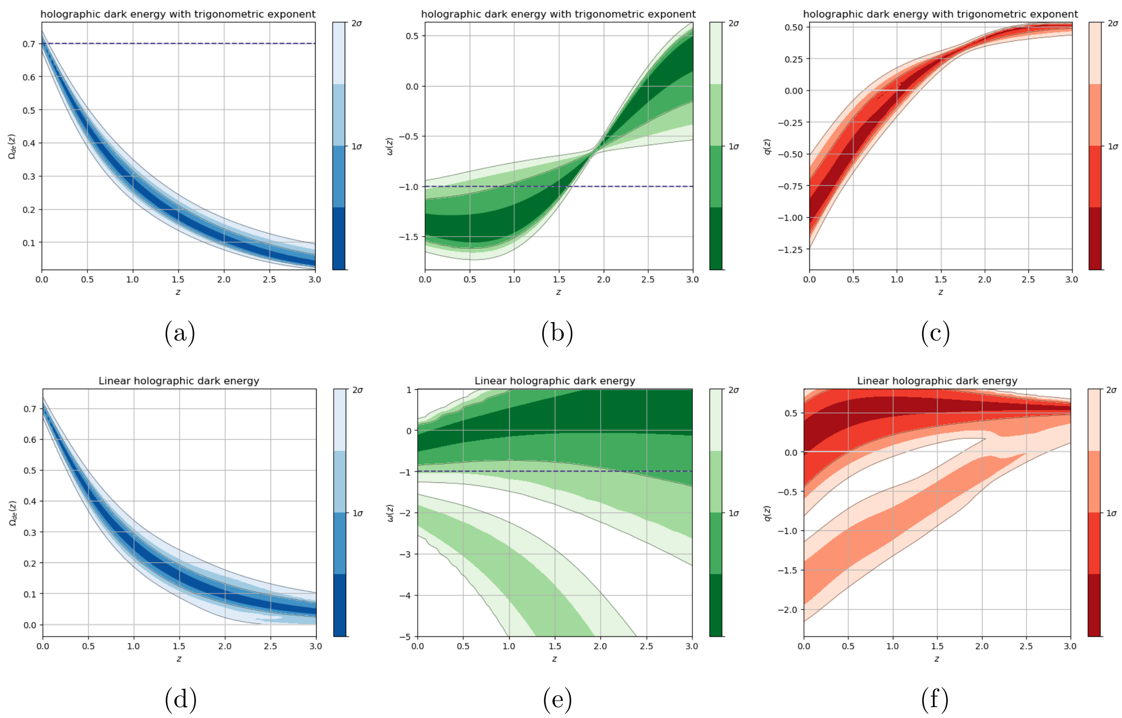

Figure 5.4: 1σ and 2σ regions for the Ω_{de}, $\omega_{de}(z)$, and $q(z)$ for linear-exponent holographic dark energy ($\mathcal{L}$HDE) and trigonometric-exponent holographic dark energy $\mathcal{S}$HDE.

on the redshift, but we can fit the oscillation's numbers that we need by modify the argument in the sin function, for example in the most general case $f(z) = k + rsin(nz)$, where n is the number of the oscillations that we need, or we can also perform an inference on this extra parameter.
Finally, the acceleration parameter given as $q(z) = -1 - \frac{\dot{H}}{H^2}$, which for our purposes is of great importance due to provides us with information about the nature of the accelerating expansion of our universe. As you remember, the case when $q > 0$ is about the decelerating universe case, suggesting that the gravitational pull of matter is decelerating the expansion of the universe. Another case is $-1 < q < 0$, in which the universe is in accelerating expansion, indicating that there is some kind of repulsive force driving the accelerated expansion, for us, it is the dark energy. The last case is for $q = 0$, this indicates a constant expansion of the universe.
The red plots are about the acceleration parameter, notice that at $z = 0$, all cases are $q < 0$, i.e., all holographic dark energy models reproduce a universe in accelerating expansion, however, only

the first three cases shown in Figure 5.3 (c), 5.3 (f) and 5.3 (i), are in the $-1 < q < 0$ region, thus, these models indicate a "moderate" accelerated expansion in cooperation with the generalized exponent holographic models, notice that for these last models, $q < -1$ in the 2σ regions, thus, is the case of super-exponential expansion, indicating a rapid acceleration that exceeds the de Sitter expansion rate.

A relevant aspect in these models, according to the plots, the models that present a greater acceleration in the sense that their phase change from an accelerated universe to an accelerated universe to a decelerated universe are the Tsallis and $\mathcal{L}$HDE models, however, the linear model has two maximal points in different regions of the a and b parameters, which does not allow this acceleration to be seen, so the Tsallis model provides a clearer view of this higher acceleration at the phase transition at $z \sim 0.5$.

Finally, be aware that the first three models, which do not have an exponential acceleration around $z \sim 0$, will eventually have a phase change as $q \longrightarrow -1$ at $z \longrightarrow -1$.

Chapter 6

Conclusion

In this thesis, we studied the impact and importance of the holographic dark energy model as a fundamental alternative and its viability through comparing observational data. Throughout the history of the expansion of the universe, there is a need for the existence of dark energy to explain the accelerated expansion of the universe. However, there are currently many dark energy models that generalize the ΛCDM model and suggest that the nature of this entity must be dynamic.
One of the main contributions of this thesis has been the inference of the holographic parameters of each model using data from observations of type Ia supernovae, the cosmic microwave background, and cosmic chronometers since the redshift associated with these observations is where dark energy is dominant.

Firstly, the results obtained confirm that holographic dark energy models are fundamental generalizations of the ΛCDM model, i.e., in the appropriate parameter limits of the models and the quantities that make up our Universe, they can perfectly reproduce this model (the equation of state parameter is recovered). For this reason, the holographic dark energy models provide additional information or corrections by introducing new parameters in each model, for example, the parameter c in all holographic dark energy models, δ in the Tsallis model $\mathcal{B}$ in the Barrow model, a and b in the linear case, k and r in the trigonometric model, all values inferred by Bayesian inference are in agreement with what is theoretically expected in each model.

By understanding how a holographic dark energy model can be constructed through the entropy bound and its relation to the energy density of the dark energy, it was possible to propose new generalizations using the exponents as a function of the redshift $f(z)$. That was done by using the Barrow model as a starting point, which are themselves generalization of the first holographic model.

These new proposals offer considerable flexibility by including new entropies that can provide a more dynamic nature to the equation of state. For example, one of the proposals is an oscillatory case to appropriate redshift regions, as suggested by the reconstructions based on the aforementioned observational data. However, the research has also identified several challenges and limitations in the implementation of generalizations of holographic dark energy models. Among these, the need for an entropy that meets the necessary properties to be a fundamental model, as described in Chapter 3, stands out. Through the results of Chapter 5, we can see those holographic dark energy models present a better fit to the observational data from Supernovae, Cosmic Chronometers, and Baryon Acoustic Oscillations in comparison with the ΛCDM model, indicated by the information criterion and the Bayes factor, the Tsallis model presents a better fit, allowing us to consider it a more comprehensive model compared to the ΛCDM model. The case of the holographic dark energy with the linear exponent is the model that possesses the minimum chi-square (58.12) among all the models studied, another important result of this model is that the values of the generalized exponent are negative, which is a theoretical impediment, but observational data prefer these values.

In conclusion, the implementation of holographic models in cosmology presents significant challenges, but their potential benefits are equally notable, as demonstrated in this work. To maximize these benefits, it is crucial to continue exploring these models, as they provide a very comprehensive and interesting alternative, and according to observational data, they offer a better fit. Future work plans to extend these models to scalar field formalisms, introduce interaction between matter and dark energy, and incorporate perturbations to obtain power spectra.

Appendices

Appendix A

Appendix A

This appendix contains the triangular plots of the cosmological parameters h ($H_0/100$), $\Omega_{b,0}h^2$, $\Omega_{m,0}$ and the holographic parameters c, $\mathcal{B}$ and δ, for the Standard, Barrow and Tsallis holographic dark energy models, also a, b, k and r for linear and trigonometric generalized exponent models, mentioned in Chapter 5, furthermore, each case is compared with the ΛCDM model. The exploration regime for the cosmological parameters are $\Omega_{m,0} \in [0.1, 0.5]$, $\Omega_{b,0}h^2 \in [0.02, 0.025]$ and $h \in [0.4, 0.9]$.

A.1 Triangular plots

A.1.1 Standard holographic dark energy

In the case of the standard holographic dark energy model, we used the prior of the holographic parameter $c \in [0.5, 2.0]$, which is based on the parameter's variation process described in Chapter 3. The posterior distributions are shown in figure A.1, and we can see a clear anticorrelation between c and h parameters, also the distributions of the cosmological parameters in both models are agreed.

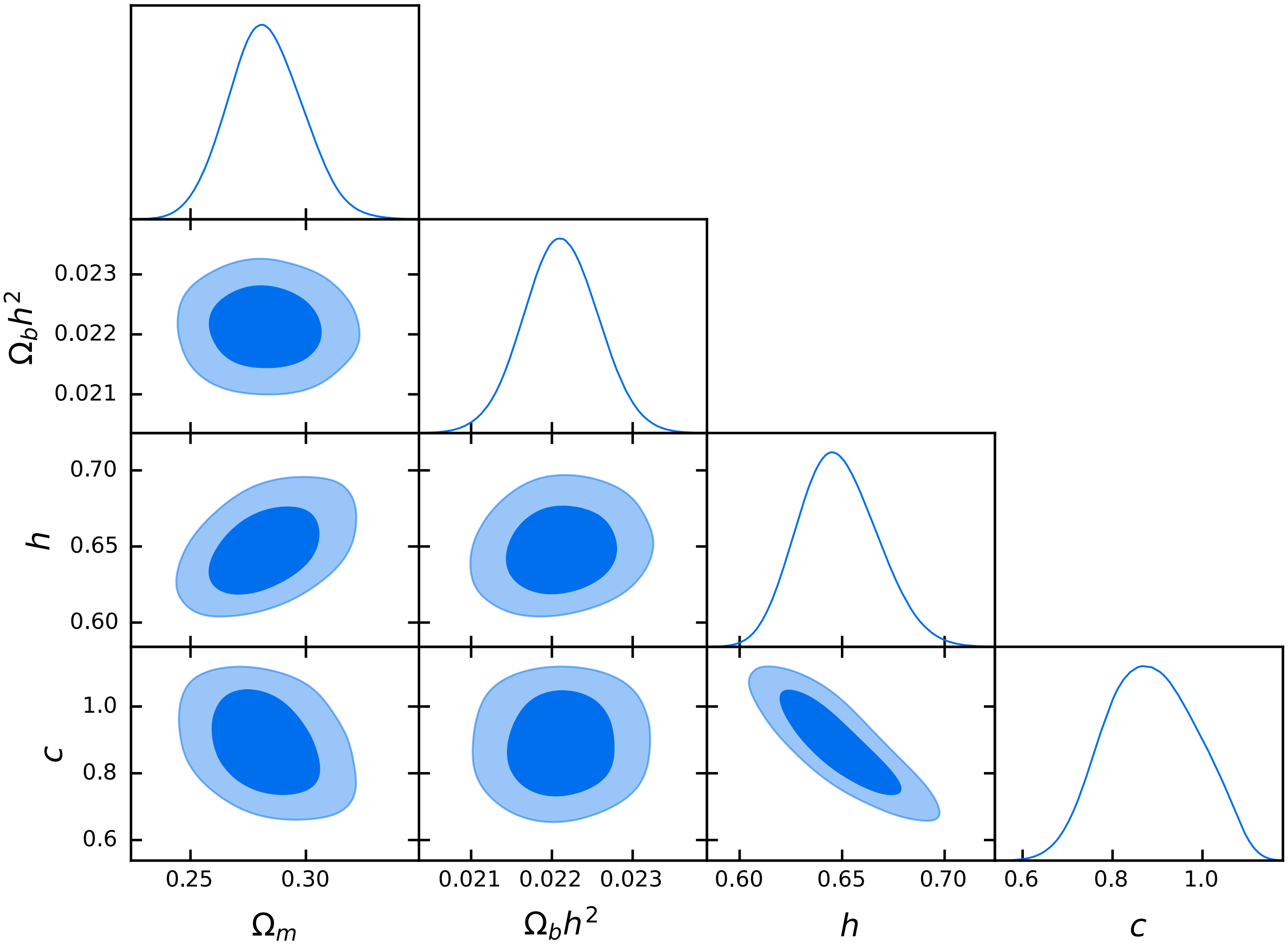

Figure A.1: Confidence regions for the holographic dark energy model.

A.1.2 Barrow's holographic dark energy

In this case, we used the same prior as in the above case for the c parameter and the prior of Barrow holographic parameter implemented was $\mathcal{B} \in [0, 1.5]$ using the fact that it should be a positive parameter in the similar parameter's variation process. In the same way as the standard holographic dark energy model, the distributions of the cosmological parameters are agreed with the distribution of the ΛCDM model as shown in figure A.2. Nevertheless, we can appreciate an anticorrelation between c and $\mathcal{B}$ holographic parameters in this case.

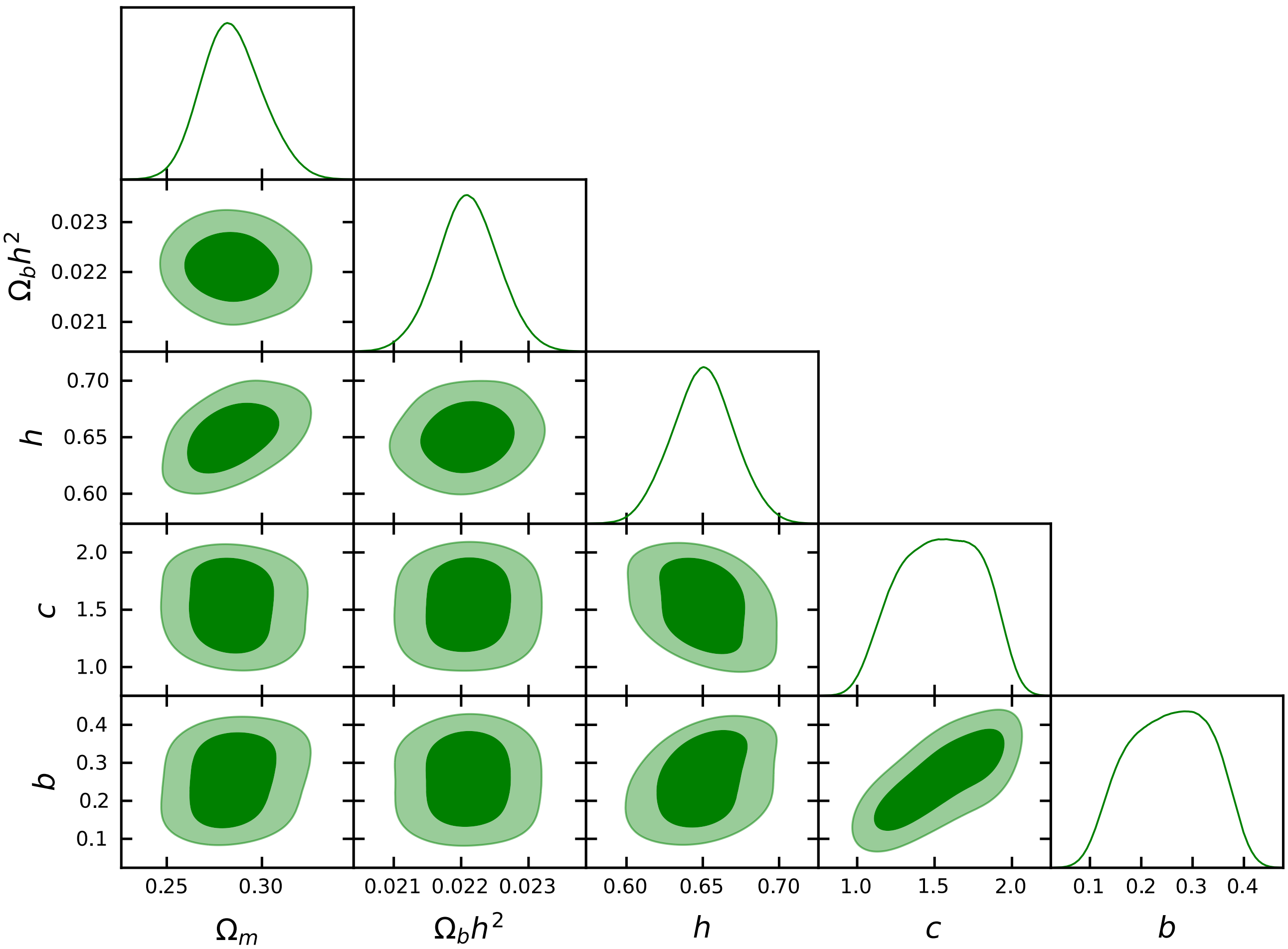

Figure A.2: Confidence regions for the Barrow's holographic dark energy model.

A.1.3 Tsallis' holographic dark energy

In the case of Tsallis holographic dark energy, we used the same prior as in the above case for the c parameter and the prior of Tsallis holographic parameter implemented was $\mathcal{B} \in [0.5, 2.0]$ using the fact that it should be a positive parameter in the similar parameter's variation process. In the same way as the standard holographic dark energy model, the distributions of the cosmological parameters are agreed with the distribution of the ΛCDM model as shown in figure A.3. Nevertheless, we can appreciate an anticorrelation between c and δ holographic parameters in this case, which is agreed with the similar result in the Barrow holographic dark energy due to both cases are constant exponent models and in precision $\delta \sim \mathcal{B}$.

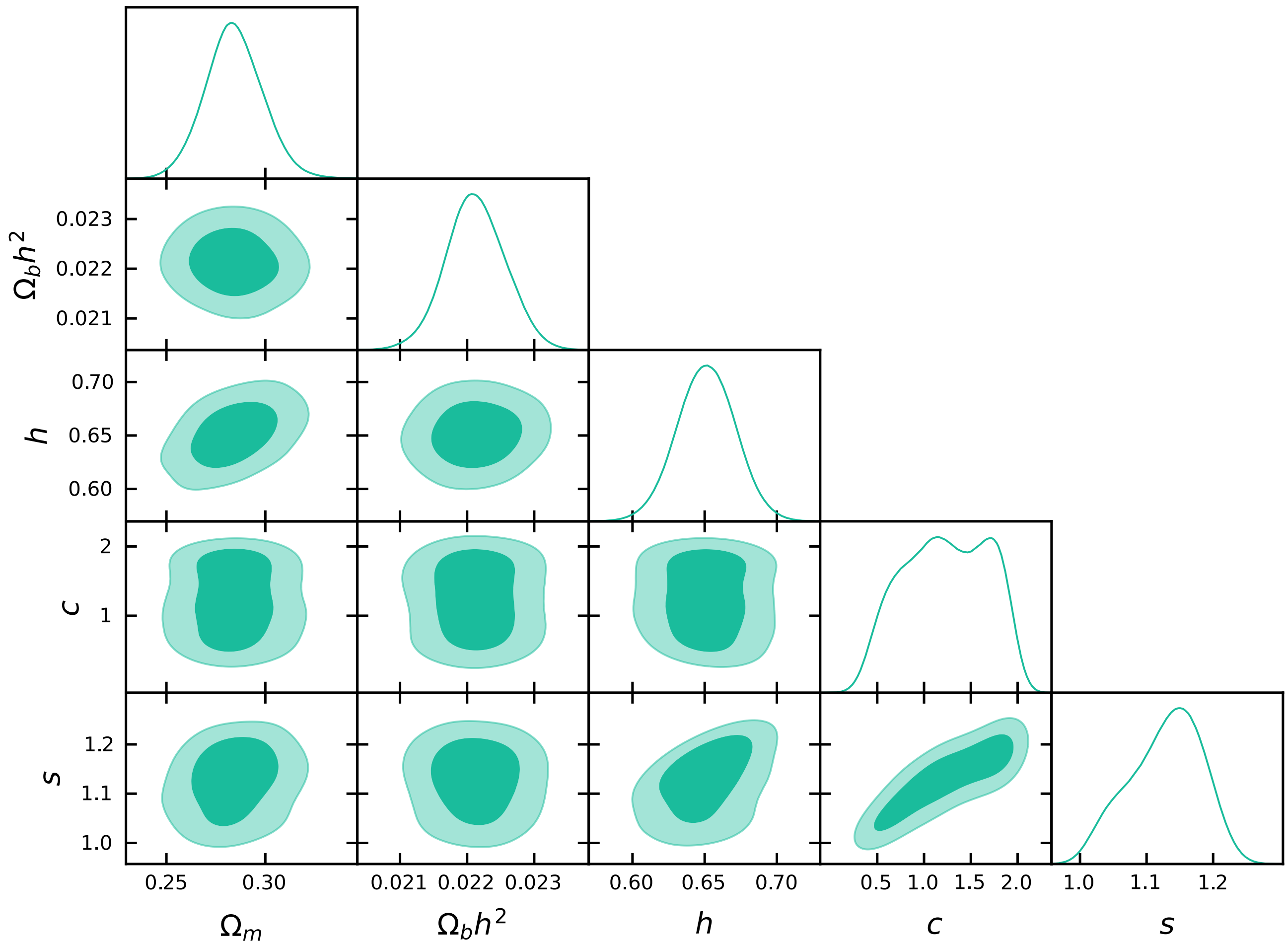

Figure A.3: Confidence regions for the Tsallis holographic dark energy model.

A.1.4 Holographic dark energy with trigonometric exponent

In the case of holographic dark energy with trigonometric exponent, we used the same prior as in the above case for the c parameter. The prior of these particular holographic parameters implemented were $a \in [0.0, 1.0]$ and $b \in [0.0, 1.0]$ using the similar parameter's variation process.

In this process, we had more liberty, and we considered the negative values of these holographic parameters, however, the associated values to negative values did not agree with data points from some observations like cosmic chronometers, thus, we discarded these values. In the same way as the standard holographic dark energy model, the distributions of the cosmological parameters are agreed with the distribution of the ΛCDM model as shown in figure A.4. Nevertheless, we can appreciate the correlation and anticorrelation behavior of the exponent's parameters with respect to the c parameter.

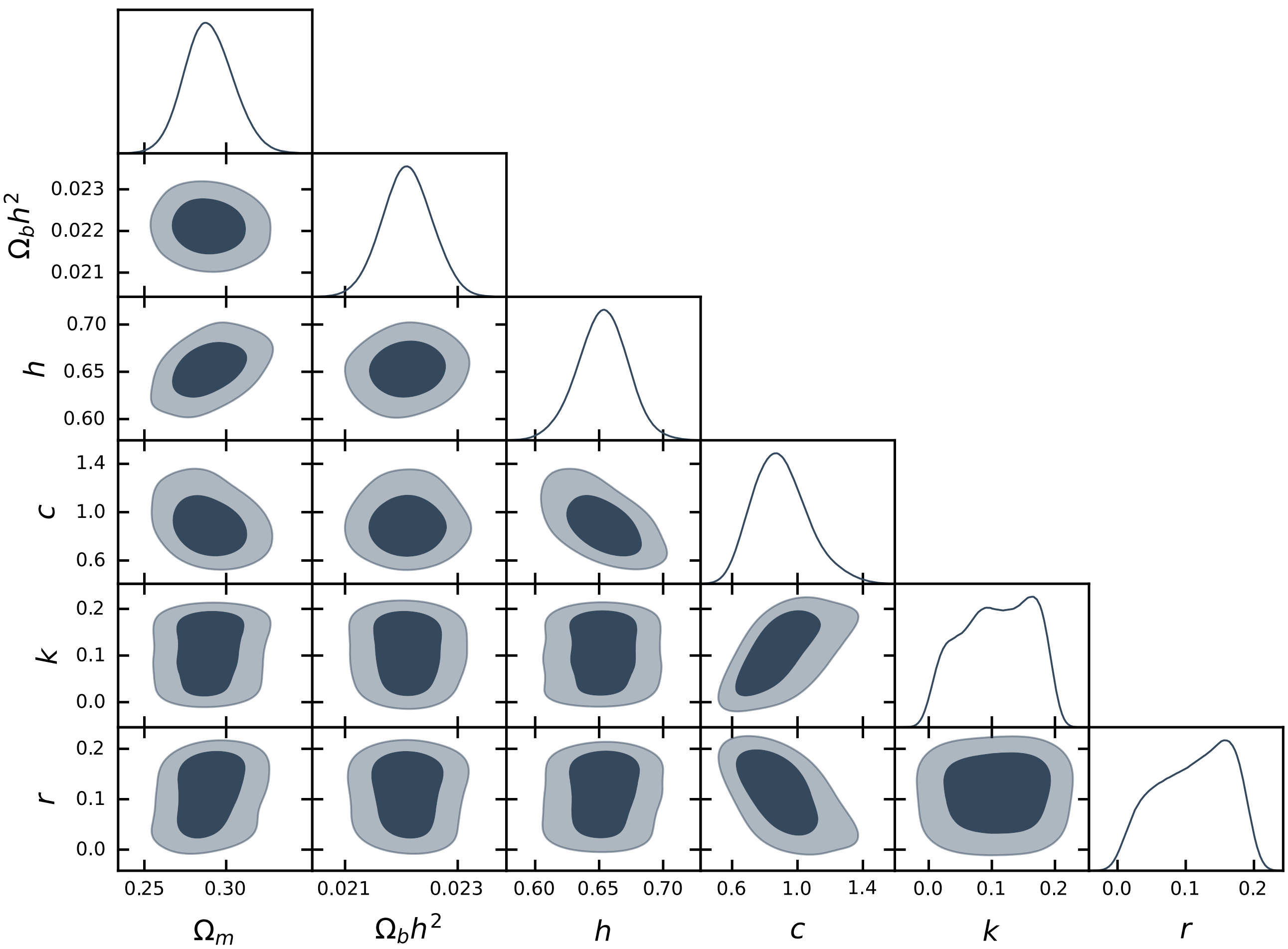

Figure A.4: Confidence regions for the holographic dark energy model with a trigonometric exponent.

A.1.5 Holographic dark energy with a linear exponent

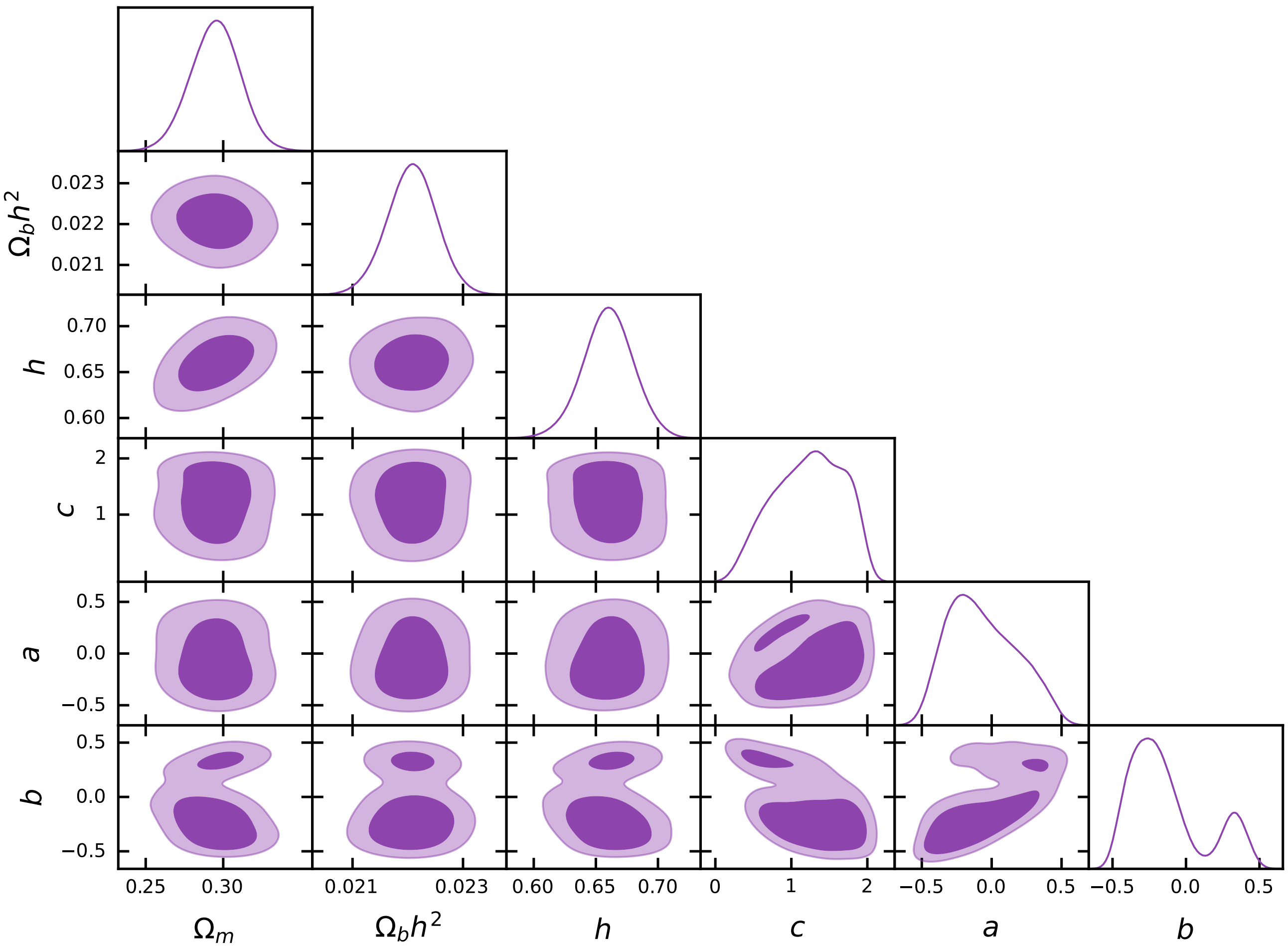

Figure A.5: Confidence regions for the holographic dark energy model with linear exponent.

Finally, in the case of holographic dark energy with linear exponent, we used the same prior as in the above case for the c parameter. The priors of these particular holographic parameters implemented were $a \in [-0.5, 0.5]$ and $b \in [-0.5, 0.5]$ using the similar parameter's variation process. In this process, we had more liberty, and we considered the negative values of these holographic parameters, however, the associated values to negative values agree with data points from some observations like cosmic chronometers, thus, we consider the negative possibility of negative values. In the same way as the standard holographic dark energy model, the distributions of the cosmological parameters are agreed with the distribution of the ΛCDM model, as shown in figure A.5. Nevertheless, we can not distinguish a correlation or anticorrelation behavior of the exponent's parameters with respect to the c parameter. Also, we can see that there are two maximums in different regions of the b parameter, and in precision, the highest peak is in the negative regime of this parameter.

Bibliography

[1] Ramos-Sanchez S. and O.M. Vidal. Relatividad para futuros fisicos. Textos contemporaneos. Copit-Arxives, 2018. ISBN: 9781938128189.

[2] S. Dodelson and F. Schmidt. Modern Cosmology. Elsevier Science, 2020. ISBN: 9780128159484. URL: https://books.google.com.mx/books?id=GGjfywEACAAJ.

[3] Sean M. Carroll. Spacetime and Geometry: An Introduction to General Relativity. San Francisco: Addison-Wesley, 2004. ISBN: 978-0805387322.

[4] Uriel Kantor. "Ancient Greek cosmology: How did the Greeks see the universe?". en. https://www.thecollector.com/cosmology-ancient-greece/. Accessed: 2024-8-6. Aug. 2023.

[5] Phillip James Edwin Peebles. Principles of physical cosmology. Vol. 27. Princeton university press, 1993.

[6] Steven Weinberg. Gravitation and Cosmology. New York: John Wiley & Sons, 1972.

[7] Planck Collaboration et al. "Planck 2018 results - VI. Cosmological parameters". In: A and A 641 (2020), A6. DOI: 10.1051/0004-6361/201833910. URL: https://doi.org/10.1051/0004-6361/201833910.

[8] Andrew R. Liddle. An introduction to modern cosmology. 1998.

[9] Saakshi Dikshit and Anwesh Bhattacharya. Cosmological Modelling of Dark Matter. Mar. 2021.

[10] Ralf Aurich et al. "The variance of the CMB temperature gradient: a new signature of a multiply connected Universe". In: (June 2021).

[11] Carlos A Bertulani. Nuclei in the Cosmos. WORLD SCIENTIFIC, 2013. DOI: 10.1142/8573. eprint: https://www.worldscientific.com/doi/pdf/10.1142/8573. URL: https://www.worldscientific.com/doi/abs/10.1142/8573.

[12] R.K. Pathria and Paul D. Beale. "Thermodynamics of the early universe". In: ed. by R.K. Pathria and Paul D. Beale. Fourth Edition. Academic Press, 2022, pp. 291–313. ISBN: 978-0-08-102692-2. DOI: https://doi.org/10.1016/B978-0-08-102692-2.00018-1. URL: https://www.sciencedirect.com/science/article/pii/B9780081026922000181.

[13] Planck Collaboration et al. "Planck 2018 results - VI. Cosmological parameters". In: A &A 641 (2020), A6. DOI: 10.1051/0004-6361/201833910. URL: https://doi.org/10.1051/0004-6361/201833910.

[14] I. Soszynski et al. The Optical Gravitational Lensing Experiment. 2009. arXiv: 0811.3636 [astro-ph]. URL: https://arxiv.org/abs/0811.3636.

[15] Saul Perlmutter. "Supernovae, dark energy, and the accelerating universe: The Status of the cosmological parameters". In: Int. J. Mod. Phys. A 15S1 (2000). Ed. by J. Jaros and Michael E. Peskin, pp. 715–739. DOI: 10.1142/S0217751X00005383.

[16] Christopher Stubbs and Yorke Brown. "Precise astronomical flux calibration and its impact on studying the nature of the dark energy". In: Modern Physics Letters A 30 (Dec. 2015), p. 1530030. DOI: 10.1142/S021773231530030X.

[17] Sean M. Carroll. Spacetime and Geometry: An Introduction to General Relativity. San Francisco: Addison-Wesley, 2004. ISBN: 978-0805387322.

[18] Steven Weinberg. "The cosmological constant problem". In: Rev. Mod. Phys. 61 (1 Jan. 1989), pp. 1–23. DOI: 10.1103/RevModPhys.61.1. URL: https://link.aps.org/doi/10.1103/RevModPhys.61.1.

[19] Jérôme Martin. "Everything you always wanted to know about the cosmological constant problem (but were afraid to ask)". In: Comptes Rendus. Physique 13.6–7 (July 2012), pp. 566–665. ISSN: 1878-1535. DOI: 10.1016/j.crhy.2012.04.008. URL: http://dx.doi.org/10.1016/j.crhy.2012.04.008.

[20] Jian-Ping Hu and Fa-Yin Wang. Hubble Tension: The Evidence of New Physics. 2023. arXiv: 2302.05709 [astro-ph.CO]. URL: https://arxiv.org/abs/2302.05709.

[21] Shinji Tsujikawa. "Quintessence: A Review". In: Classical and Quantum Gravity 30 (Nov. 2013). DOI: 10.1088/0264-9381/30/21/214003.

[22] Eric Linder. "Exploring the Expansion History of the Universe". In: Physical review letters 90 (Apr. 2003), p. 091301. DOI: 10.1103/PhysRevLett.90.091301.

[23] Jr. E. M. Barboza and J. S. Alcaniz. "A parametric model for dark energy". In: Phys. Lett. B 666 (2008), pp. 415–419. DOI: 10.1016/j.physletb.2008.08.012. arXiv: 0805.1713 [astro-ph].

[24] Shinji Tsujikawa. "Quintessence: A Review". In: Classical and Quantum Gravity 30 (Nov. 2013). DOI: 10.1088/0264-9381/30/21/214003.

[25] Vivian Poulin, Tristan L. Smith, and Tanvi Karwal. "The Ups and Downs of Early Dark Energy solutions to the Hubble tension: A review of models, hints and constraints circa 2023". In: Physics of the Dark Universe 42 (2023), p. 101348. ISSN: 2212-6864. DOI: https://doi.org/10.1016/j.dark.2023.101348. URL: https://www.sciencedirect.com/science/article/pii/S2212686423001826.

[26] Marcel A. van der Westhuizen and Amare Abebe. "Interacting dark energy: clarifying the cosmological implications and viability conditions". In: JCAP 01 (2024), p. 048. DOI: 10.1088/1475-7516/2024/01/048. arXiv: 2302.11949 [gr-qc].

[27] B Wang et al. "Dark matter and dark energy interactions: theoretical challenges, cosmological implications and observational signatures". In: Reports on Progress in Physics 79.9 (Aug. 2016), p. 096901. ISSN: 1361-6633. DOI: 10.1088/0034-4885/79/9/096901. URL: http://dx.doi.org/10.1088/0034-4885/79/9/096901.

[28] Weiqiang Yang et al. "Tale of stable interacting dark energy, observational signatures, and the H0 tension". In: Journal of Cosmology and Astroparticle Physics 2018.09 (Sept. 2018), p. 019. DOI: 10.1088/1475-7516/2018/09/019. URL: https://dx.doi.org/10.1088/1475-7516/2018/09/019.

[29] Matteo Lucca. "Dark energy–dark matter interactions as a solution to the S8 tension". In: Physics of the Dark Universe 34 (2021), p. 100899. ISSN: 2212-6864. DOI: https://doi.org/10.1016/j.dark.2021.100899. URL: https://www.sciencedirect.com/science/article/pii/S2212686421001291.

[30] Kim V. Berghaus et al. “Dark energy radiation”. In: Physical Review D 104.8 (Oct. 2021). ISSN: 2470-0029. DOI: 10.1103/physrevd.104.083520. URL: http://dx.doi.org/10.1103/PhysRevD.104.083520.

[31] Kim V. Berghaus et al. “The Cosmology of Dark Energy Radiation”. In: (Nov. 2023). arXiv: 2311.08638 [hep-ph].

[32] Kim V. Berghaus et al. “Dark energy radiation”. In: Phys. Rev. D 104.8 (2021), p. 083520. DOI: 10.1103/PhysRevD.104.083520. arXiv: 2012.10549 [hep-ph].

[33] Kim V. Berghaus et al. The Cosmology of Dark Energy Radiation. 2024. arXiv: 2311.08638 [hep-ph]. URL: https://arxiv.org/abs/2311.08638.

[34] Lárus Thorlacius and Thordur Jonsson. M-theory and quantum geometry. Jan. 2000, p. 471. ISBN: 978-0-7923-6475-7. DOI: 10.1007/978-94-011-4303-5.

[35] Andrew Cohen, David Kaplan, and Ann Nelson. “Effective Field Theory, Black Holes, and the Cosmological Constant”. In: Physical Review Letters 82 (June 1999). DOI: 10.1103/PhysRevLett.82.4971.

[36] Shuang Wang, Yi Wang, and Miao Li. “Holographic dark energy”. In: Physics Reports 696 (2017). Holographic Dark Energy, pp. 1–57. ISSN: 0370-1573. DOI: https://doi.org/10.1016/j.physrep.2017.06.003. URL: https://www.sciencedirect.com/science/article/pii/S0370157317301564.

[37] Stephen D.H. Hsu. “Entropy bounds and dark energy”. In: Physics Letters B 594.1 (2004), pp. 13–16. ISSN: 0370-2693. DOI: https://doi.org/10.1016/j.physletb.2004.05.020. URL: https://www.sciencedirect.com/science/article/pii/S0370269304007658.

[38] Miao Li. “A model of holographic dark energy”. In: Physics Letters B 603.1 (2004), pp. 1–5. ISSN: 0370-2693. DOI: https://doi.org/10.1016/j.physletb.2004.10.014. URL: https://www.sciencedirect.com/science/article/pii/S0370269304014388.

[39] Eoin Ó Colgáin and M M Sheikh-Jabbari. “A critique of holographic dark energy”. In: Classical and Quantum Gravity 38.17 (Aug. 2021), p. 177001. DOI: 10.1088/1361-6382/ac1504. URL: https://dx.doi.org/10.1088/1361-6382/ac1504.

[40] Qing-Guo Huang and Miao Li. "The Holographic Dark Energy in a Non-flat Universe". In: Journal of Cosmology and Astroparticle Physics 2004 (Apr. 2004). DOI: 10.1088/1475-7516/2004/08/013.

[41] Yun-gui Gong, Bin Wang, and Yuan-Zhong Zhang. "The Holographic dark energy revisited". In: Phys. Rev. D 72 (2005), p. 043510. DOI: 10.1103/PhysRevD.72.043510. arXiv: hep-th/0412218.

[42] Mubasher Jamil, Emmanuel N. Saridakis, and M. R. Setare. "Holographic dark energy with varying gravitational constant". In: Phys. Lett. B 679 (2009), pp. 172–176. DOI: 10.1016/j.physletb.2009.07.048. arXiv: 0906.2847 [hep-th].

[43] Marek Biesiada and Beata Malec. "A new white dwarf constraint on the rate of change of the gravitational constant". In: Monthly Notices of the Royal Astronomical Society 350.2 (May 2004), pp. 644–648. ISSN: 1365-2966. DOI: 10.1111/j.1365-2966.2004.07677.x. URL: http://dx.doi.org/10.1111/j.1365-2966.2004.07677.x.

[44] Craig J. Copi, Adam N. Davis, and Lawrence M. Krauss. "New Nucleosynthesis Constraint on the Variation of G". In: Physical Review Letters 92.17 (2004), p. 171301. DOI: 10.1103/PhysRevLett.92.171301.

[45] Yun-He Li et al. "Holographic dark energy in a universe with spatial curvature and massive neutrinos." In: Journal of Cosmology and Astroparticle Physics 2013.02 (Feb. 2013), pp. 033–033. ISSN: 1475-7516. DOI: 10.1088/1475-7516/2013/02/033. URL: http://dx.doi.org/10.1088/1475-7516/2013/02/033.

[46] Miao Li, Chunshan Lin, and Yi Wang. "Some issues concerning holographic dark energy". In: Journal of Cosmology and Astroparticle Physics 2008.05 (May 2008), p. 023. DOI: 10.1088/1475-7516/2008/05/023. URL: https://dx.doi.org/10.1088/1475-7516/2008/05/023.

[47] Bin Chen, Miao Li, and Yi Wang. "Inflation with Holographic Dark Energy". In: Nuclear Physics B 774 (July 2007), pp. 256–267. DOI: 10.1016/j.nuclphysb.2007.04.007.

[48] Yungui Gong. "Extended holographic dark energy". In: Physical Review D 70.6 (Sept. 2004). ISSN: 1550-2368. DOI: 10.1103/physrevd.70.064029. URL: http://dx.doi.org/10.1103/PhysRevD.70.064029.

[49] B Guberina, R Horvat, and H Štefančić. "Hint for quintessence-like scalars from holographic dark energy". In: Journal of Cosmology and Astroparticle Physics 2005.05 (May 2005), pp. 001–001. ISSN: 1475-7516. DOI: 10.1088/1475-7516/2005/05/001. URL: http://dx.doi.org/10.1088/1475-7516/2005/05/001.

[50] Xin Zhang. "Dynamical vacuum energy, holographic quintom, and the reconstruction of scalar-field dark energy". In: Phys. Rev. D 74 (10 Nov. 2006), p. 103505. DOI: 10.1103/PhysRevD.74.103505. URL: https://link.aps.org/doi/10.1103/PhysRevD.74.103505.

[51] Shin'Ichi Nojiri and Valerio Faraoni. How fundamental is entropy? Jan. 2022.

[52] Emmanuel N. Saridakis. "Barrow holographic dark energy". In: Phys. Rev. D 102.12 (2020), p. 123525. DOI: 10.1103/PhysRevD.102.123525. arXiv: 2005.04115 [gr-qc].

[53] John D. Barrow. "The Area of a Rough Black Hole". In: Phys. Lett. B 808 (2020), p. 135643. DOI: 10.1016/j.physletb.2020.135643. arXiv: 2004.09444 [gr-qc].

[54] Emmanuel N. Saridakis and Spyros Basilakos. "The generalized second law of thermodynamics with Barrow entropy". In: The European Physical Journal C 81.7 (July 2021), p. 644. ISSN: 1434-6052. DOI: 10.1140/epjc/s10052-021-09431-y. URL: https://doi.org/10.1140/epjc/s10052-021-09431-y.

[55] C. Tsallis. "Possible generalization of Boltzmann-Gibbs statistics". In: Journal of Statistical Physics 52 (July 1988), pp. 479–487. DOI: 10.1007/BF01016429.

[56] Saridakis et al. "Holographic dark energy through Tsallis entropy". In: Journal of Cosmology and A.P. 2018.12 (Dec. 2018), p. 012. DOI: 10.1088/1475-7516/2018/12/012. URL: https://dx.doi.org/10.1088/1475-7516/2018/12/012.

[57] Ahmad Sheykhi and Maral Sahebi Hamedan. "Holographic Dark Energy in Modified Barrow Cosmology". In: Entropy 25.4 (2023). ISSN: 1099-4300. DOI: 10.3390/e25040569. URL: https://www.mdpi.com/1099-4300/25/4/569.

[58] Luis A. Escamilla et al. "Oscillations in the Dark?" In: (Mar. 2024). arXiv: 2404.00181 [astro-ph.CO].

[59] Luis E. Padilla et al. “Cosmological Parameter Inference with Bayesian Statistics”. In: Universe 7.7 (June 2021), p. 213. ISSN: 2218-1997. DOI: 10.3390/universe7070213. URL: http://dx.doi.org/10.3390/universe7070213.

[60] Christian P. Robert. The Metropolis-Hastings algorithm. 2016. arXiv: 1504.01896 [stat.CO]. URL: https://arxiv.org/abs/1504.01896.

[61] Johannes Buchner. “Nested sampling methods”. In: Statistic Surveys 17 (2023), pp. 169–215.

[62] Johannes Buchner. “Nested sampling methods”. In: (Jan. 2021). DOI: 10.1214/23-ss144. arXiv: 2101.09675 [stat.CO].

[63] M. Moresco et al. “Improved constraints on the expansion rate of the Universe up to z = 1.1 from the spectroscopic evolution of cosmic chronometers”. In: Journal of Cosmology and A. P. 2012.08 (Aug. 2012), p. 006. DOI: 10.1088/1475-7516/2012/08/006. URL: https://dx.doi.org/10.1088/1475-7516/2012/08/006.

[64] Joan Simon, Licia Verde, and Raul Jimenez. “Constraints on the redshift dependence of the dark energy potential”. In: Phys. Rev. D 71 (12 June 2005), p. 123001. DOI: 10.1103/PhysRevD.71.123001. URL: https://link.aps.org/doi/10.1103/PhysRevD.71.123001.

[65] Stern Daniel et al. “Cosmic chronometers: constraining the equation of state of dark energy. I: H(z) measurements”. In: Journal of Cosmology and Astroparticle Physics 2010.02 (Feb. 2010), p. 008. DOI: 10.1088/1475-7516/2010/02/008. URL: https://dx.doi.org/10.1088/1475-7516/2010/02/008.

[66] Michele Moresco et al. “A 6 percent measurement of the Hubble parameter at z = 0.45: direct evidence of the epoch of cosmic re-acceleration”. In: Journal of Cosmology and A.P. 2016.05 (May 2016), pp. 014–014. ISSN: 1475-7516. DOI: 10.1088/1475-7516/2016/05/014. URL: http://dx.doi.org/10.1088/1475-7516/2016/05/014.

[67] M. Betoule et al. “Improved cosmological constraints from a joint analysis of the SDSS-II and SNLS supernova samples”. In: Astronomy and Astrophysics - A&A 568 (2014), A22. DOI: 10.1051/0004-6361/201423413. URL: https://cea.hal.science/cea-01271043.

[68] Éric Aubourg et al. “Cosmological implications of baryon acoustic oscillation measurements”. In: Phys. Rev. D 92 (12 Dec. 2015), p. 123516. DOI: 10.1103/PhysRevD.92.123516. URL: https://link.aps.org/doi/10.1103/PhysRevD.92.123516.

[69] Antony Lewis. GetDist: a Python package for analysing Monte Carlo samples. 2019. arXiv: 1910.13970 [astro-ph.IM]. URL: https://arxiv.org/abs/1910.13970.

[70] Will Handley. "fgivenx: Functional Posterior Plotter". In: The Journal of Open Source Software 3.28 (Aug. 2018). DOI: 10.21105/joss.00849. URL: http://dx.doi.org/10.21105/joss.00849.